Stage dependent differential influence of metabolic and structural networks on memory across Alzheimer's disease continuum

Kok Pin Ng FRCP[1,4,5*], Xing Qian PhD[2*], Kwun Kei Ng PhD[2], Fang Ji PhD[2], Pedro Rosa-Neto MD PhD[7,8], Serge Gauthier MD FRCPC[8], Nagaendran Kandiah FRCP[1,4,5], Juan Helen Zhou PhD[2,3,4,6] for the Alzheimer's Disease Neuroimaging Initiative[#]

[1]Department of Neurology, National Neuroscience Institute, Singapore, Singapore

[2]Centre for Sleep and Cognition and Centre for Translational MR Research, Yong Loo Lin School of Medicine, National University of Singapore, Singapore, Singapore

[3]Department of Electrical and Computer Engineering, National University of Singapore, Singapore, Singapore

[4]Duke-NUS Medical School, Singapore, Singapore

[5]Lee Kong Chian School of Medicine, Nanyang Technological University Singapore, Singapore, Singapore

[6]Integrative Sciences and Engineering Programme (ISEP), National University of Singapore, Singapore, Singapore

[7]Translational Neuroimaging Laboratory, McGill University Research Centre for Studies in Aging, Alzheimer's Disease Research Unit, Douglas Research Institute, Le Centre intégré universitaire de santé et de services sociaux (CIUSSS) de l'Ouest-de-l'Île-de-Montréal, and Departments of Neurology, Neurosurgery, Psychiatry, Pharmacology and Therapeutics, McGill University, Montreal, Quebec, Canada

[8]Montreal Neurological Institute, McGill University, Montreal, Quebec, Canada

*Both authors contributed equally to the manuscript

#Data used in the preparation of this article were obtained from the Alzheimer's Disease Neuroimaging Initiative (ADNI) database (adni.loni.usc.edu). As such, the investigators within the ADNI contributed to the design and implementation of ADNI and/or provided data but did not participate in the analysis or writing of this report. A complete listing of ADNI investigators can be found at http://adni.loni.usc.edu/wp-content/uploads/how_to_apply/ADNI_Acknowledgement_List.pdf

Corresponding author:
Juan Helen Zhou, Ph.D.
Address: Tahir Foundation Building (MD1), 12 Science Drive 2, #13-05, National University of Singapore, Singapore 117549
Tel: (65) 66014918
Fax: (65) 62218685
Email: helen.zhou@nus.edu.sg

Running title: Network-memory association trajectory

Keywords: metabolic and structural networks; memory; amyloid; tau, Alzheimer's disease, mild cognitive impairment

Abbreviations:

A = amyloid-beta plaques; AD = Alzheimer's disease; ADNI = Alzheimer's Disease Neuroimaging Initiative; ANG = angular gyrus; ANOVA = analysis of variance; Aβ = amyloid-beta; CDR = clinical dementia rating; CN = cognitively normal; DLPFC = dorsolateral prefrontal cortex; DMN = default mode network; ECN = executive control network; FC = functional

connectivity; FDG = [18F]Fluorodeoxyglucose; FWE = family-wise error; FWHM = Full-Width at Half-Maximum; GM = grey matter; GMV = grey matter volume; HIP = hippocampus; ICV = intracranial volume; INS = insular; LV = latent variable; MCI = mild cognitive impairment; MMSE = mini-mental state examination; MNI = Montreal Neurological Institute; mPFC = medial prefrontal cortex; MPRAGE = magnetization-prepare rapid-acquisition gradient echo; N = neurodegeneration; PCC = posterior cingulate cortex; PLS = partial least squares; PPC = posterior parietal cortex; SN = salience network; SOB = sum of boxes; SPGR = sagittal inversion-recovery spoiled gradient-recalled; SUVR = standardized uptake value ratio; SVC = sparse varying coefficient; T = tau neurofibrillary tangles accumulation; VBM = voxel-based morphometry

ABSTRACT

Background: Large-scale neuronal network breakdown underlies memory impairment in Alzheimer's disease (AD). However, the differential trajectories of the relationships between network organization and memory across pathology and cognitive stages in AD remain elusive. We determined whether and how the influences of individual-level structural and metabolic covariance network integrity on memory varied with amyloid pathology across clinical stages without assuming a constant relationship. **Methods:** 708 participants from the Alzheimer's Disease Neuroimaging Initiative were studied. Individual-level structural and metabolic covariance scores in higher-level cognitive and hippocampal networks were derived from magnetic resonance imaging and [^{18}F]fluorodeoxyglucose positron emission tomography using seed-based partial least square analyses. The non-linear associations between network scores and memory across cognitive stages in each pathology group were examined using sparse varying coefficient modelling. **Results:** We showed that the associations of memory with structural and metabolic networks in the hippocampal and default mode regions exhibited pathology-dependent differential trajectories across cognitive stages using sparse varying coefficient modelling. In amyloid pathology group, there was an early influence of hippocampal structural network deterioration on memory impairment in the preclinical stage, and a biphasic influence of the angular gyrus-seeded default mode network metabolism on memory in both preclinical and dementia stages. In non- amyloid pathology groups, in contrast, the trajectory of the hippocampus-memory association was opposite and weaker overall, while no metabolism covariance networks were related to memory. Key findings were replicated in a larger cohort of 1280 participants. **Conclusions:** Our findings highlight potential windows of early intervention targeting network breakdown at the preclinical AD stage.

INTRODUCTION

Alzheimer's disease (AD) is a neurodegenerative disease that is characterized by neuropathological accumulation of amyloid-beta (Aβ) plaques (A), intraneuronal tau neurofibrillary tangles (T), and neurodegeneration (N) in the brain [1, 2]. While AD is traditionally a clinical-pathologic condition, the emerging development of biomarkers to profile AD pathophysiology has led to the proposal of AD as a biological construct based on the AT(N) system [3, 4]. The incorporation of the AT(N) classification into the clinical continuum will offer robust disease staging by combining both pathophysiological and cognitive phenotypes which span from cognitively intact to mild cognitive impairment (MCI) before progressing to the dementia stage [5]. Studies have suggested that Aβ is the first to become abnormal in AD, followed by downstream pathophysiological changes of tauopathy, neurodegeneration, and cognitive impairment [6, 7, 8]. While neurodegeneration is widely associated with worse cognitive impairment in neurocognitive disorders, it remains unknown whether the influence of neurodegeneration on cognitive function varies with AD biomarkers status and across the AD continuum.

Neurodegeneration represents neuronal injury in the forms of cerebral grey matter (GM) atrophy and hypometabolism. In AD, it is widely postulated that Aβ triggers tau-mediated toxicity leading to AD-type neurodegeneration in brain regions such as the hippocampus, the precuneus and posterior cingulate cortex, bilateral angular gyrus, and medial temporal lobes [9, 10, 11, 12]. Recently, amyloid and tau pathologies are also shown to have a synergistic effect on AD-type hypometabolism, involving the basal and mesial temporal, orbitofrontal, and anterior and posterior cingulate cortices [13, 14]. However, neurodegeneration may also occur prior to incident amyloid positivity [15] and be influenced by the loss of microtubule stabilizing function and toxic effects of tau pathology, independent of amyloid pathology [16].

Advancement in brain network analysis offers insights into the functional effects of AD pathophysiology on cognitive changes. Work from our group has demonstrated that AD pathophysiologies compromise brain sturcture and function systematically by capitalizing on the intrinsic connectivities among brain regions [17]. Accumulating evidence suggests that AD pathological deposition around neurons which impairs synaptic communication, leads to specific large-scale brain intrinsic network disorganization [18, 19]. Decreased functional connectivity in the default mode network (DMN) derived from resting state functional MRI is well-described in MCI and AD [20, 21, 22, 23, 24], while aberrant loss of functional connectivity in other higher-order cognitive networks such as the executive control network (ECN) and salience network (SN) are being increasingly reported [22, 25, 26].

Brain networks can also be constructed based on similarity in GM structure and metabolism between brain areas across individuals, known as the GM structural and metabolic covariance network respectively [27, 28, 29]. Both structural and metabolic covariance networks show convergent patterns with the intrinsic connectivity network in healthy individuals and mirror GM atrophy patterns in distinct neurodegenerative disorders [18, 27, 30]. Using this approach, a recent study revealed differential patterns of structural covariance networks within different amyloid pathology groups classified by CSF $A\beta_{1-42}$ and P-tau_{181} levels [31]. However, existing studies on the GM structural and metabolic covariance networks were largely reliant on group-level correlation maps of cortical morphology and metabolism, which cannot be used to infer individual differences in cognition. It is postulated that network analysis at the individual level will allow direct evaluation of each individual's structural and metabolic covariance networks, hence providing deeper understanding on the effects of brain networks on cognitive performances [32]. For instance, a cube-based correlation approach to calculate the individual GM networks by computing intracortical

similarities in GM morphology [33] showed that single-subject GM graph properties were associated with individual differences of clinical progression in AD [34, 35, 36, 37]. A network template perturbation approach was also introduced to construct an individual differential SCN using regional GM volume, though it required reference models derived from a group of normal control subjects [38]. Nevertheless, the relationships between changes in individual-level network-based neurodegeneration across different amyloid pathology groups and cognitive stages, and their influence on memory impairment, remain unclear.

The influence of cerebral GM loss and [^{18}F]Fluorodeoxyglucose (FDG) hypometabolism on cognitive function in AD has often been modelled as a linear relationship [39, 40]. However, emerging evidence suggests that structural and metabolic abnormalities in AD may follow a sigmoidal curve trajectory with an initial period of acceleration and subsequent deceleration [7, 41, 42]. While the dynamic effects of AD biomarkers on worsening cognition can be better modelled by sigmoid-shaped curves rather than a constant across disease stages [43], it remains largely unknown how brain structural and metabolic networks will influence cognition decline differentially in individuals stratified into different pathology groups and cognitive stages. Once these trajectories are defined across the AD continuum and subgroups, they can potentially highlight windows of opportunity for targeted intervention at the appropriate cognitive stages to improve disease outcomes.

To cover these gaps, we sought to determine the differential associations of brain metabolism and GM structural networks with memory function using a neurodegeneration covariance network approach, among cognitively normal (CN), mild cognitive impairment (MCI), and probable AD individuals stratified by their A and T biomarker status. We used the seed partial least squares (PLS) method [44] to evaluate the individual-level brain network integrity. We

employed the sparse varying coefficient (SVC) model which does not assume a constant relationship between brain measures and cognitive performance over different cognitive stages [45, 46, 47]. Besides capturing the possible nonlinear brain-cognition relationship, SVC also allows the selection of significant predictors with the LASSO sparse penalty while eliminating the contribution of the less important predictors. We hypothesized that individual-level brain metabolic and structural network integrity would be non-linearly associated with memory performance across the AD continuum and such trajectories would vary depending on the presence of amyloid and tau protein deposition. Based on our previous findings [21, 22, 48], we further hypothesized that the posterior DMN and the medial temporal lobe regions would play an early and dominant role affecting the memory performance in individuals with amyloid pathology.

Our study provides first evidence that both hippocampal structural and angular gyrus metabolic network integrity contributed to memory performance in the early cognitively normal stage in individuals with amyloid deposition. However, in the amyloid positive individuals with dementia, only the angular gyrus metabolic network dominated the memory-network association. Amyloid negative individuals did not have such patterns. These findings characterize the dynamic influence of brain structural and metabolic networks on memory function across the AD continuum and underscore the importance of early intervention targeting neuronal dysfunction in the preclinical AD stage to improve memory outcomes.

RESULTS

Group differences in brain metabolic and structural covariance networks

We selected 812 participants (232 CN, 413 MCI and 167 probable AD) from the Alzheimer's Disease Neuroimaging Initiative (ADNI) database with 3T T1-weighted MRI and [^{18}F]FDG PET

scans to define seed regions for brain network derivation (Fig. 1, step 1). As our study focused on memory and AD pathology, we chose to study the individual-level structural and metabolic covariance within higher-order cognitive networks such as DMN, SN, ECN as well as the hippocampus (HIP)-based memory network [49, 50]. We defined a set of 12 seed regions to derive these covariance networks on the basis that they have been shown to reliably produce the relevant network across imaging modalities. Specifically, the DMN included bilateral angular gyrus (ANG), posterior cingulate cortex (PCC), and medial prefrontal cortex (mPFC); the SN included bilateral anterior insular (INS); the ECN included bilateral dorsolateral prefrontal cortex (DLPFC) and posterior parietal cortex (PPC); the memory network included bilateral HIP. The seed coordinates were determined based on the group comparisons of the grey matter volume (GMV) probability and glucose metabolic spatial maps between CN and probable AD individuals (Supplementary Table 3, see details in Methods).

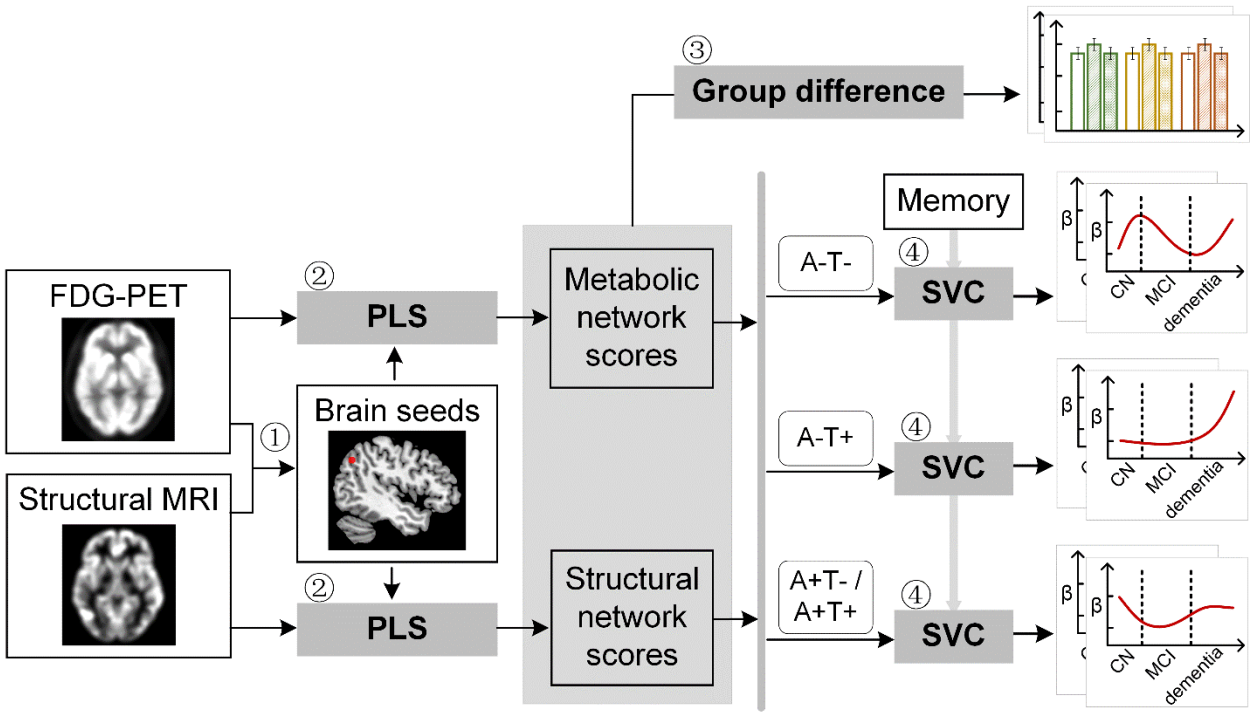

Figure 1. Study design schematic. 708 participants with either healthy cognition (CN), mild cognitive impairment (MCI) or dementia were studied. Twelve brain seeds covering the key regions of hippocampus, the default mode network, the executive control network, and salience network were defined based on hypometabolism (via FDG) and grey matter atrophy (via MRI) patterns in all patients with probable AD compared to CN (**step 1**). Using seed-based partial least square (PLS) analysis (**step 2**), the covariance patterns in metabolism and GMV maps were identified and used to derive the individual-level brain metabolic network scores and structural network scores for each seed. The group difference was evaluated between different cognitive stages and pathology groups (**step 3**). We then investigated the differential stage-dependent associations between these key brain network scores with memory performance in each of the three pathology groups (A-T-, A-T+, and A+T-/A+T+) separately using sparse varying coefficient (SVC) modelling (step 4). Abbreviations: A = Aβ; T = tau; '-' = negative; '+' = positive.

To derive brain structural and metabolic networks from individuals with and without amyloid pathology, we further identified 708 out of the existing 812 participants who underwent neuropsychological assessments, and lumbar puncture, in addition to [^{18}F]FDG PET and T1-weighted MRI scans to form the main dataset (Table 1). Using seed PLS (Fig. 1, step 2, see details in Methods), we identified the structural and metabolic covariance network patterns associated with each seed at the group-level (Fig. 2A and Fig. 3A). We projected the original individual GMV and metabolic maps onto the covariance network maps to derive the individual brain structural or metabolic network scores, which reflected how strongly each brain network pattern was manifested in the individual's metabolic and structural brain networks.

First, we compared the brain metabolic and structural network scores between different pathology groups and cognitive stages (Fig. 1, step 3). At the same cognitive stage, amyloid positive CN and MCI individuals had lower metabolic and structural network scores than those amyloid negative CN and MCI individuals for all the networks (Fig. 2B & 3B). No such difference was observed at the dementia stage.

Table 1. Subject demographics for the main study cohort.

	A-T-			A-T+			A+T-/A+T+		
	CN	**MCI**	**probable AD**	**CN**	**MCI**	**probable AD**	**CN**	**MCI**	**probable AD**
N	30	74	4	80	75	7	85	225	128
Age, y	65.12~85.16	56.08~88.51	69.56~90.50	56.53~84.47	55.15~88.83	60.79~80.76	60.19~90.08	55.38~91.57	55.96~90.46
	72.24±4.54	69.78±7.20^{d}	77.37±9.11^{m}	71.95±5.87	70.21±8.16	74.57±7.70	75.37±6.59	73.17±6.93	74.12±8.19
Gender (M/F)	12/18	39/35	4/0	45/35	38/37	6/1	37/48	127/98	72/56
Handedness	29/1	60/14	4/0	69/11	67/8	7/0	79/6	203/22	118/10
(R/L)									
Education, y	16.63±2.68	16.45±2.59	17.50±1.29	16.88±2.67	16.00±2.65	16.71±2.43	16.34±2.36	16.12±2.74	15.78±2.71
APOE e4 (+/-)	6/24	16/58	0/4	16/64	17/58	1/6	38/47^{md}	140/85^{cd}	93/35^{cm}
Memory	1.28±0.66^{md}	0.75±0.64^{cd}	-0.12±0.68^{cm}	1.17±0.57^{md}	0.55±0.62^{cd}	-0.40±0.67^{cm}	0.97±0.63^{md}	0.20±0.63^{cd}	-0.87±0.53^{cm}
MMSE	28.70±1.68^{d}	28.62±1.31^{d}	25.75±2.36^{cm}	29.15±0.99^{md}	28.29±1.64^{cd}	23.86±2.19^{cm}	29.02±1.17^{md}	27.81±1.86^{cd}	23.21±2.24^{cm}
CDR-SOB	0.02±0.09^{md}	1.22±0.60^{cd}	4.38±3.04^{cm}	0.05±0.15^{md}	1.20±0.76^{cd}	4.57±1.40^{cm}	0.05±0.17^{md}	1.53±0.90^{cd}	4.64±1.70^{cm}
ICV	1523.77±	1520.05±	1540.83±	1554.01±	1559.14±	1566.75±	1524.87±	1558.61±	1549.78±
	152.57	127.78	36.50	128.10	147.96	221.76	148.29	148.25	163.05

Note: Data on age are range and mean ± SD. Data on education, ICV, and memory are mean ± SD. Data on memory are in z-scores. Abbreviations: CN = cognitively normal; MCI = mild cognitive impairment; AD = Alzheimer's disease; A= β-amyloid; T = tau; '+' = positive; '-' = negative; y = years; M = male; F = female; R = right; L = left; MMSE = Mini-Mental State Exam; CDR-SOB = Clinical Dementia Rating Sum of Box; ICV = intracranial volume. Superscripts ('^{c}', '^{m}', '^{d}') represent significant group difference with CN, MCI and probable AD respectively.

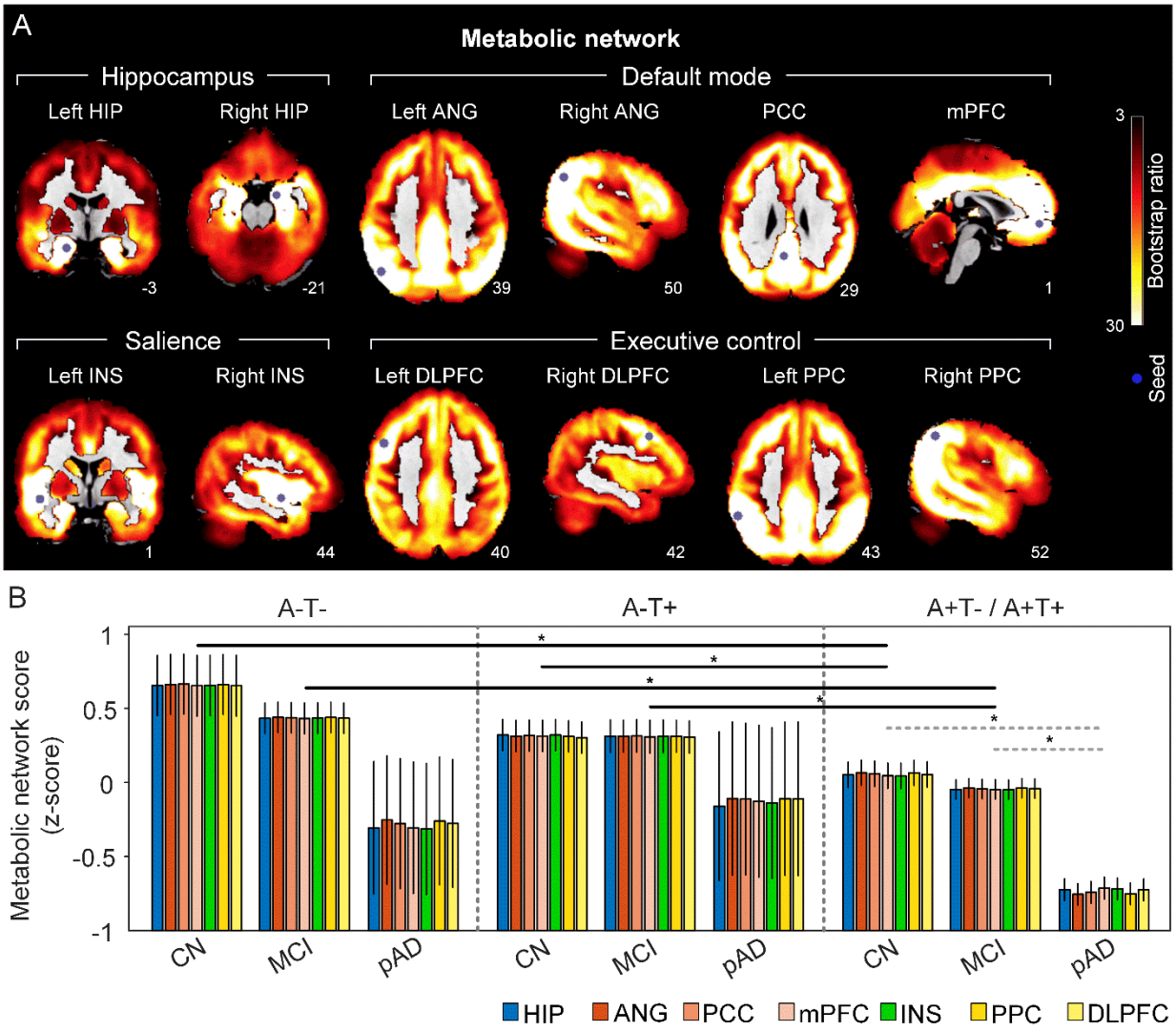

Figure 2. The integrity of brain metabolic networks in participants with and without amyloid pathology across cognitive stages. A. Brain slices of metabolic covariance networks associated with each brain seed defined from FDG-PET data highlighted in blue circles. Brain metabolic network resemabled canonical brain networks. The intensity of colorbar represents bootstrap ratios, derived from dividing the weight of the singular-vector by the bootstrapped standard error. B. Individual-level brain metabolic network scores were lower in individuals with worse cognition and amyloid pathology. Summary of individual-level metabolic network scores (mean ± SD) were presented in bar charts. '*' indicates significant group difference (ANOVA; $p < 0.05$). Thick lines indicate group differences in brain network scores between different cognitive stages (grey dashed lines) or pathology groups (dark lines). Abbreviations: HIP = hippocampus; ANG = angular gyrus; PCC = posterior cingulate cortex; mPFC = media prefrontal cortex; INS = insular; DLPFC = dorsolateral prefrontal cortex; PPC = posterior parietal cortex; CN = cognitively normal; MCI = mild cognitive impairment; pAD = probable AD; A= β-amyloid; T = tau; '+' = positive; '-' = negative; HIP = hippocampus; ANG = angular gyrus; PCC = posterior cingulate cortex; mPFC =

media prefrontal cortex; INS = insular; DLPFC = dorsolateral prefrontal cortex; PPC = posterior parietal cortex.

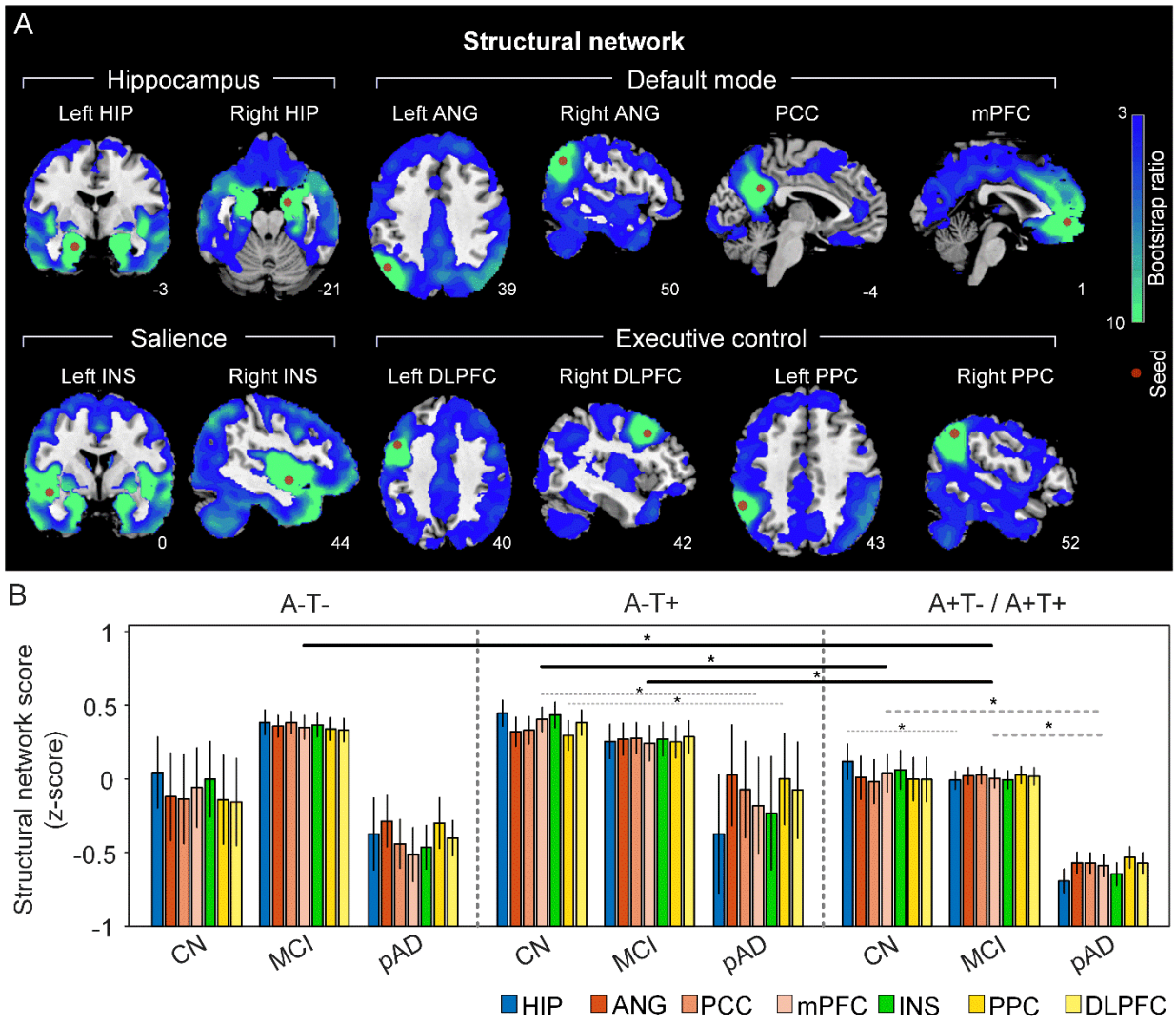

Figure 3. The integrity of brain structural networks in participants with and without amyloid pathology across cognitive stages. A. brain slices of structural covariance networks associated with each brain seed defined from GMV data highlighted in blue circles. The intensity of colorbar represents bootstrap ratios, derived from dividing the weight of the singular-vector by the bootstrapped standard error. B. Individual-level brain structural network scores were lower in individuals with worse cognition and amyloid pathology. Summary of individual-level structural network scores (mean ± SD) were presented in bar charts. '*' indicates significant group difference (ANOVA; $p<0.05$). Thick lines indicate group differences in all brain network scores between different cognitive stages (grey dashed lines) or pathology groups (dark lines). Abbreviations: HIP = hippocampus; ANG = angular gyrus; PCC = posterior cingulate cortex; mPFC = media prefrontal cortex; INS = insular; DLPFC = dorsolateral prefrontal cortex; PPC = posterior parietal cortex;

CN = cognitively normal; MCI = mild cognitive impairment; pAD = probable AD; A= β-amyloid; T = tau; '+' = positive; '-' = negative; HIP = hippocampus; ANG = angular gyrus; PCC = posterior cingulate cortex; mPFC = media prefrontal cortex; INS = insular; DLPFC = dorsolateral prefrontal cortex; PPC = posterior parietal cortex.

Within the same pathology group, we observed slightly different patterns in structural and metabolic networks. Specifically, in participants with amyloid pathology (A+T-/A+T+), the probable AD group had lower metabolic and structural network scores than the CN and MCI groups in all the networks (Fig. 2B right and 3B right). The amyloid positive MCI group had comparable metabolic network scores but lower structural HIP-based memory network scores than the amyloid positive CN group. In contrast, participants without amyloid and tau pathology (A-T-) did not show any differences in both metabolic and structural networks across the three cognitive stages (Fig. 2B left and 3B left). Interestingly, participants with tau pathology (A-T+) had no cognitive stage-related differences in all metabolic networks, while the tau positive dementia group had lower structural integrity in the mPFC-based anterior DMN and PPC-based ECN than the tau positive CN group (Fig. 2B middle and 3B middle).

Divergent stage-dependent trajectories of the association between hippocampal structural network integrity and memory performance in the three pathology groups

Next, we sought to determine the differential nonlinear trajectories of the association between brain network integrity and memory impairment in different pathology groups across the three cognitive stages using the SVC model (Fig. 1, step 4) [45]. Note that we did not assume a constant relationship here; instead, the network-memory association could vary across cognitive stages. Instead of analyzing each brain measure in separate models, the SVC analysis allows all variables

to be entered as predictors in the same multivariate model, with the identification of the most important predictors and the elimination of the less important predictors (i.e. feature selection) implemented by minimizing the penalized least squares function.

To characterize the possible stage-dependent tracjectories using SVC modelling, we ordered the participants by their cognitive stages (i.e., CN → MCI → dementia; Supplementary Fig. 4 A) in each of the three pathology groups (A-/T-, A-/T+ and A+T-/A+T+). Within each stage, the participants were then ordered by their global cognition or dementia severity (i.e., no impairment → severe impairment). Specifically, the participants within the CN group were ordered by decreasing MMSE scores, while the participants within the MCI and dementia groups were ordered by increasing CDR-sum of boxes (SOB) scores. Participants with the same MMSE or CDR-SOB scores were further ordered by increasing age (i.e., young → old). Ordered participants were distributed evenly into bins (i.e., 10 subjects/bin). In our SVC models, the dependent variable was the ADNI memory composite score. Predictors included all the 14 FDG/GMV regional network scores with gender, education years, *APOE* ε4, intracranial volume (ICV), and scanning site as nuisance variables. We performed the SVC modelling for each pathology group separately to find the key predictors and the trajectories of their associations with memory along the disease progression (see details in Methods).

The SVC models identified the HIP-based structural memory network score as a key predictor of memory impairment in all three pathology groups (Fig. 4A and 5A). We found that the lower HIP structural network scores, the lower the ADNI-mem scores (indicated by positive beta coefficient). The strength of this association was higher (i.e., higher beta coefficient) in the amyloid pathology group than the other two A- groups.

More importantly, not only was the relationship between the HIP structural network and memory performance non-linearly dependent on cognitive stages as hypothesized, but such non-linear trajectories were also different across the three pathology groups (Fig. 4A and 5A). Specifically, in the amyloid pathology group, the strength of this association was highest in early CN stage, and decreased from late CN to early MCI stage (Fig. 4A, left). The strength of this association remained stable in MCI and then decreased in the dementia stage.

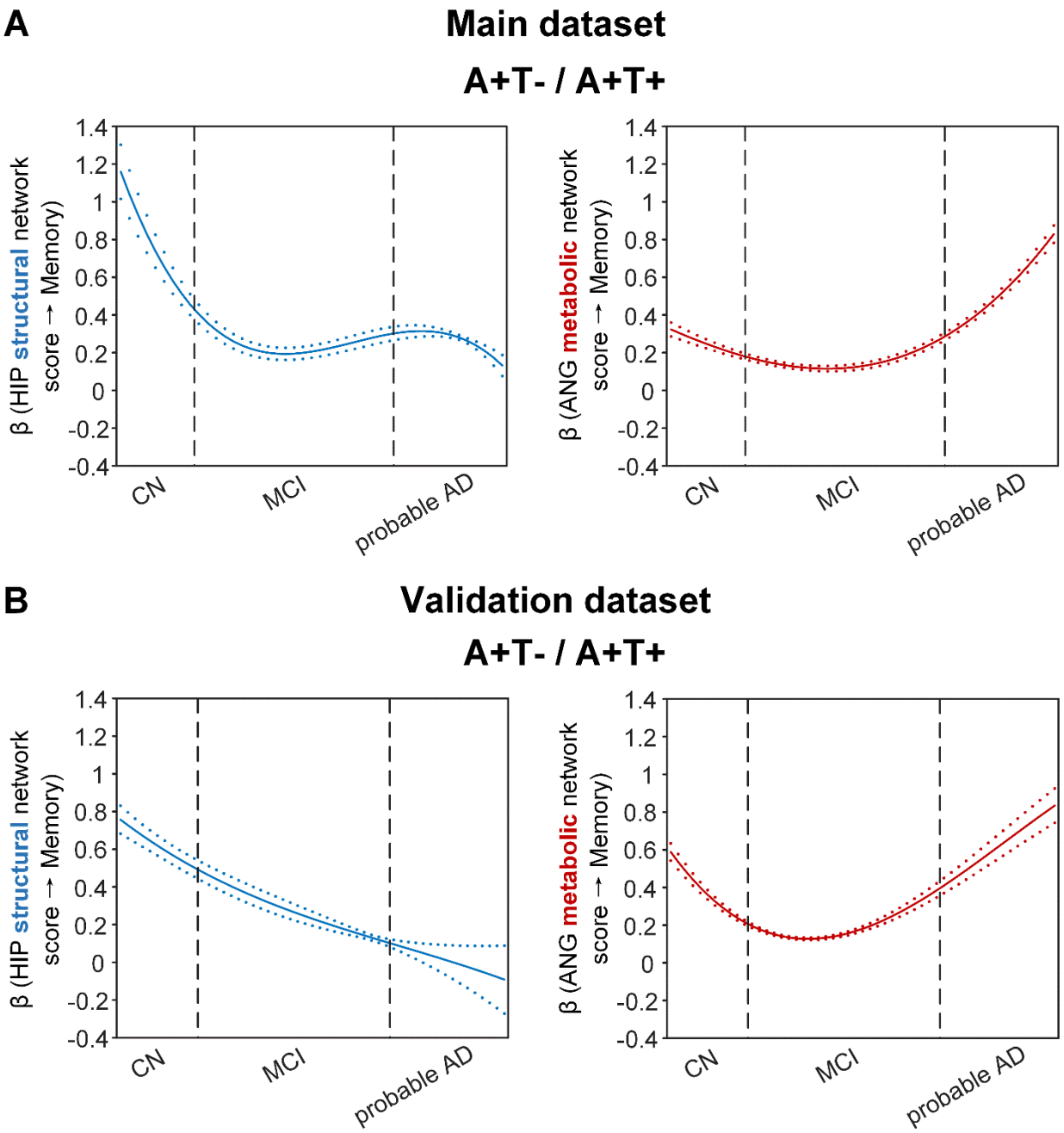

Figure 4. Brain metabolic and structural networks had differential stage-dependent associations with memory in amyloid positive individuals. Data from the main (panel A) and validation dataset (panel B) exhibited consistent stage-dependent memory-network association trajectory from cognitively normal to dementia stage in participants with amyloid pathology (i.e. A+T-/A+T+ group**)**. Both hippocampal-seeded structural network (left, in blue) and angular gyrus-seeded default mode metabolic network (right, in red) integrity contributed significantly to memory performance in early cognitively normal stage. Such impact decreased in MCI stage for both metabolic and structural networks. In contrast, only the metabolic network had a major

influence on memory in late dementia stage. Solid curves represent the mean associations (beta coefficients) of brain network scores with memory as a function of advancing AD continuum estimated from 100 replicates. The dashed curves represent the point-wise 2* standard errors of the solid curves estimated from 100 replicates. The participants were ordered by their cognitive stages (i.e., CN → MCI → probable AD). Within each cognitive stage, the participants were then ordered by general cognition (MMSE for CN) or dementia severity (CDR for MCI and dementia) (i.e., no impairment → severe impairment). Participants with the same level of impairment/severity were further ordered by increasing age (i.e., young → old). Ordered participants were distributed evenly into bins (i.e., 10 subjects/bin). Abbreviations: CN = cognitively normal; MCI = mild cognitive impairment; HIP = hippocampus; ANG = angular gyrus.

The two amyloid negative groups had the opposite pattern of the amyloid positive group (Fig. 5A). Specifically, in the A-T- group, the strength of the association between the HIP structural network and memory performance was lowest in early CN stage and increased in the late CN stage. It then remained stable in the MCI stage before a further increase in the dementia stage. Similarly, in the A-T+ group, the strength of such association was low in the CN stage and gradually increased in the MCI stage, reaching the highest in the late MCI and dementia stage.

Our findings suggest that the influence of the HIP-based structural network integrity on memory performance begins early in the preclinical AD stage and the strength of this influence gradually decreased as the cognitive stages progress. On the other hand, the influence of the HIP network integrity on memory is weaker in individuals without Aβ pathology and peaks in the dementia stage. The stronger hippocampus-memory association in the preclinical AD stage supports the current strategy of early intervention to attain better cognitive outcomes.

Furthermore, demographical and genetic variables such as gender, education years and *APOE* ε4 genotype showed differential stage- and pathology-dependent associations with memory performance (Supplementary Fig. 6). Females and fewer years of education were associated with memory impairment in A-/T- and A-/T+ groups respectively. These associations were highest in

the early CN stage and gradually decreased in late CN stage before increasing in the late MCI and probable AD stages. In contrast, females, fewer years of education and *APOE* ε4 carriers in the amyloid pathology group were associated with memory impairment with a differential trajectory (i.e., highest in the early CN stage and gradually decreased afterwards), although the strength of this association was relatively lower overall compared to those in the A-/T- and A-/T+ groups.

Stage-dependent association between angular gyrus metabolic network integrity and memory performance in amyloid pathology group

The SVC models identified the angular gyrus-based (ANG) metabolic network score (i.e., DMN) to be associated with memory impairment only in the amyloid pathology group (Fig. 4A, right). We found that the lower the ANG metabolic network score, the lower the ADNI-mem score. This suggested that a breakdown in the ANG-based metabolic covariance network was related to worse memory performance in the amyloid pathology group only. A non-linear relationship was also observed between the ANG metabolic covariance network and memory performance across different cognitive stages. The strength of this relationship showed an early peak in early CN and gradually decreased in the late CN and MCI stages, before increasing in late MCI/dementia stage again.

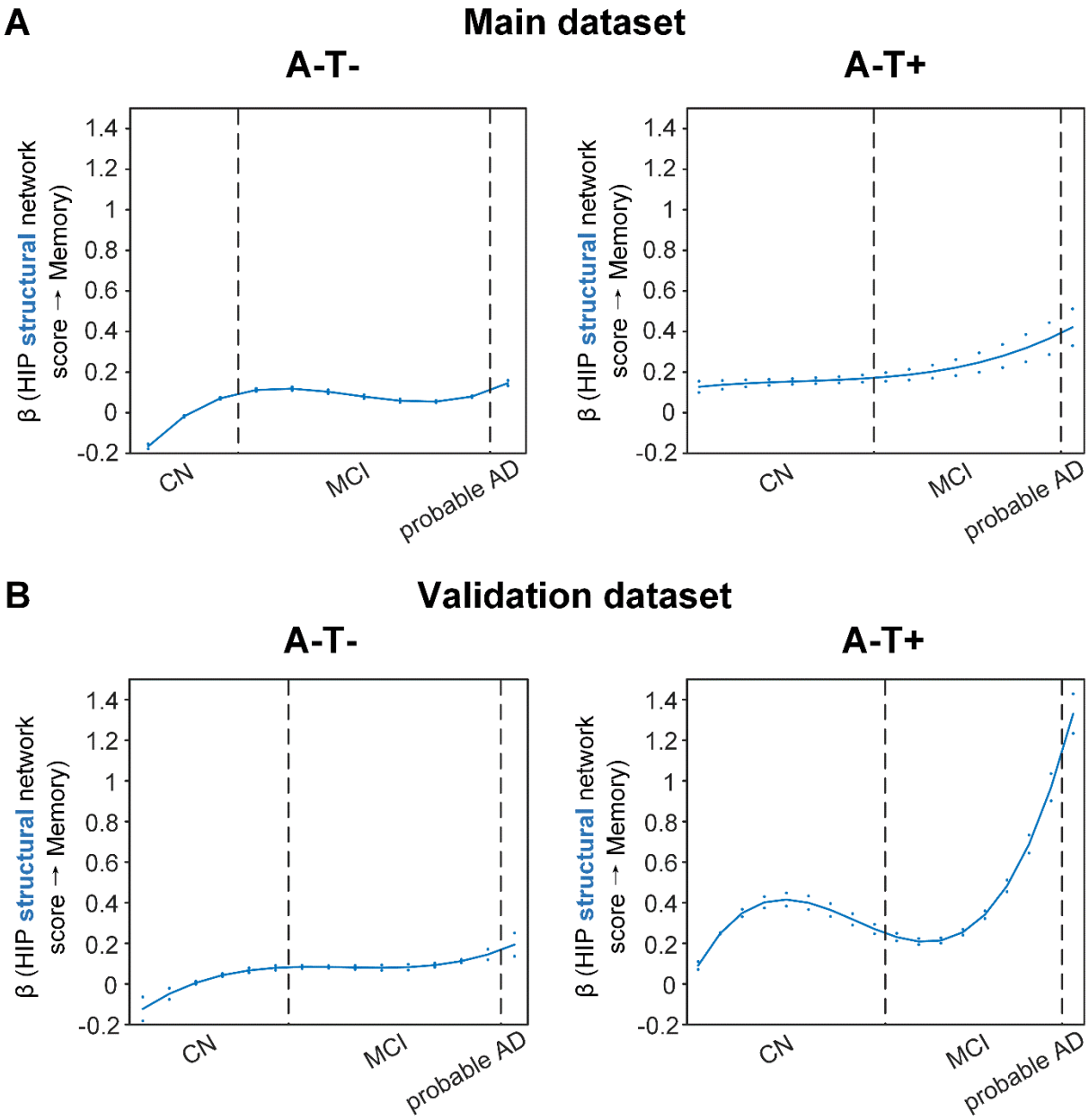

Figure 5. Stage-dependent association of brain hippocampal structural network with memory performance in A-T- and A-T+ pathology groups. Data from the main (panel A) and validation dataset (panel B) exhibited consistent stage-dependent memory-network association trajectory from cognitively normal stage to dementia stage in participants with A-T- and A-T+ pathology. The hippocampus-memory association was much weaker overall in non-amyloid/non-tau and tau only groups compared to amyloid positive group (Figure 4). The memory-network association was the lowest in early cognitively normal stage and gradually increased with clinical progression in both groups, while the tau only group had stronger associations in dementia stage. Solid curves represent the mean associations (beta coefficients) of brain network scores with memory as a function of advancing AD continuum estimated from 100 replicates. The dashed

curves represent the point-wise 2* standard errors of the solid curves estimated from 100 replicates. The participants were ordered by their cognitive stages (i.e., CN → MCI → probable AD). Within each cognitive stage, the participants were then ordered by general cognition (MMSE for CN) or dementia severity (CDR for MCI and dementia) (i.e., no impairment → severe impairment). Participants with the same same level of impairment/severity were further ordered by increasing age (i.e., young → old). Ordered participants were distributed evenly into bins (i.e., 10 subjects/bin). Abbreviations: CN = cognitively normal; MCI = mild cognitive impairment; HIP = hippocampus.

Our findings are in line with the current literature which show that decreased glucose uptake in the ANG is associated with worse cognitive performance in the later stages of AD. In addition, we extend this field by demonstrating the early influence of the ANG-based metabolic covariance network (mirroring the DMN) for memory performance in the preclinical AD stage. This suggests that early metabolic dysfunction of the ANG and the extended DMN may predispose individuals with preclinical AD to be more vulnerable to memory impairment.

Replication in the validation dataset

To test if the above findings from the main dataset can be replicated, we repeated the same analyses using another larger validation dataset. We added an additional 468 individuals who underwent 1.5T T1-weighted MRI scans and [^{18}F]FDG PET. With the original main dataset of 812 participants, we had 1280 participants in total for brain seed definition (Fig. 1, step 1). Out of 1280 participants, 859 participants had the same neuropsychological assessments, lumbar puncture for the following analyses (Fig. 1, steps 2 & 3, Supplementary Table 3). The field strength (i.e., 1.5-T or 3-T) was further included as an additional nuisance variable for analyses on the validation dataset. We performed the same PLS-SVC analyses and replicated most of our key findings (Fig. 4B and 5B, Supplementary Fig. 2, 3, and 7, see Supplementary Results). Specifically, the HIP-

based structural memory network and the ANG-based metabolic default mode network scores were associated with memory impairment in the respective pathology groups with similar beta curves as the main dataset. Furthermore, these observations remained robust when the analyses were performed using the alternative ordering strategy of merging both MCI and dementia stages (Supplementary Fig. 5 & 8).

High specificity of the SVC model

Lastly, we evaluated the specificity of the established SVC models using permutation tests. For each null SVC model using the permuted datasets, the frequency distributions of variable selection (i.e., the total times of selection as the key predictor of memory scores within the 100 permuted datasets) appeared random (see Supplementary Fig. 9). As the selected variables in our main findings were not favoured over the other variables in the null models, this indicated the high specificity of the SVC models that were built on the original dataset.

DISCUSSION

This study revealed differential associations of brain structural and glucose metabolism covariance networks with memory performance across the cognitive stages of CN, MCI and probable AD in individuals stratified by Aβ and tau pathologies. Rather than assuming a constant brain-memory association, we demonstrated that brain structural and metabolic network integrity had non-linear associations with memory performance across different cognitive stages; such trajectories exhibited opposing patterns in individuals with and without amyloid pathology. A lower HIP structural network score was associated with a lower ADNI-mem score and among individuals with amyloid pathology, the strength of this relationship was greatest in early CN and decreased

in subsequent cognitive stages. In contrast, the strength of this association was lower and the trajectory was opposite in those with both tau-only and non-amyloid/non-tau pathology. An association between the breakdown of the default mode metabolic network seeded at the ANG with memory deficit was also observed in individuals with amyloid pathology, with the strength of this association peaking in early CN and decreasing gradually before rebounding in the late MCI/dementia stage. Our findings support the AD biomarker hypothetical models by characterizing the non-linear influence of brain structural and metabolic networks on memory function across the AD continuum, hence paving the way for early interventions and stage-dependent remedies to modify disease trajectory and improve clinical outcomes.

Early influence of hippocampal structural network deterioration on memory impairment in asymptomatic amyloid-positive individuals

The HIP structural network is identified to be associated with memory impairment in all three pathology groups which is consistent with the role that the hippocampus plays in memory cognitive domain [51, 52]. However, the peak influence of the HIP structural integrity on memory differed among the three pathology groups. The early peak of the association at the CN stage in the amyloid pathology group suggests an early influence of the hippocampal structural network integrity on memory performance in the preclinical AD stage. Our findings are in line with a recent study that compared MRI brain structure models of normal and AD participants across the entire lifespan, showing that the AD model for hippocampus diverged early from normal aging trajectory [53]. Accumulating evidence also suggests hippocampal volume and thickness as early imaging correlates of verbal memory in preclinical AD [54]. Furthermore, in a cohort of CN individuals, decreased CSF Aβ42 was associated with hippocampal loss and poorer performance on episodic

memory [55], while an early effect of Aβ on memory mediated by hippocampal atrophy has been demonstrated in non-demented older individuals [56, 57, 58]. These evidence supports our findings of the early influence of structural covariance breakdown in the hippocampal networks on memory performance in the preclinical AD stage.

In our cohort with amyloid pathology, the strength of the association between HIP structural network and memory gradually decreased in the MCI and dementia stages. This suggests that the HIP structural network integrity plays a lesser role on memory performance as the cognitive stages progress. Given that memory impairment is expected to worsen as the cognitive stage progresses, we postulate that structural networks outside the hippocampal/temporal lobes may be increasingly affected while the influence from the hippocampal-based memory network decreases. Indeed, the hippocampus system is well connected to various cortical brain regions in processing memory information [59] and together with brain structures such as the prefrontal cortex make up a large-scale network to support encoding and retrieval of episodic memory [60]. While the medial temporal lobe is well known to be affected early on in the AD process, gray matter regions outside the medial temporal lobes are gradually implicated as the disease progresses to MCI and dementia [54]. Atrophy in brain regions within the DMN such as the precuneus and the posterior cingulate gyrus are shown to be associated with episodic memory impairment [61] and decreased inferior frontal gyrus volume is associated with verbal memory decline in MCI patients who converted to AD over time [62].

Angular gyrus-seeded default mode network metabolic deterioration plays a key role in memory deficit in the asymptomatic and dementia stages of AD

While impaired glucose uptake in the ANG is consistently shown to be an important feature for predicting memory and executive functioning performance in the later stages of AD [63, 64], our present findings provide further insights into the early critical role of ANG-based metabolic covariance network for intact memory (i.e., earlier peak of beta) in the preclinical AD stage. The ANG, located in the posterior part of the inferior parietal lobule, is one of the major connector hubs that links different subsystems such as the DMN [20, 65] that are affected by AD pathophysiology, and is involved in verbal working memory [66, 67] and episodic memory retrieval [68]. The role of ANG in memory performance is also implicated by its strong connectivity with the hippocampal system [67] that is critical in episodic and declarative memory functions [51]. Furthermore, a recent study showed that Aβ aggregation within the brain's DMN is associated with regional hypometabolism in distant but functionally connected brain regions, including the inferior parietal cortices where the ANG is located [69]. Therefore, early malfunctioning of the ANG, as indicated by aberrant metabolic network patterns in our study, may predispose CN individuals with amyloid pathology to a more vulnerable memory system.

Interestingly, we observed that the relationship between ANG-based metabolic covariance network and memory performance gradually decreased in the late CN and MCI stages before increasing in the dementia stage. We postulate that this may represent a metabolic compensatory mechanism in the MCI stage as a manifestation of cognitive reserve to preserve memory function, which has been proposed in AD functional connectivity (FC) studies. Among amnestic MCI individuals, increased FC compared to controls was found within the DMN and between DMN and brain networks such as the frontoparietal control and dorsal attention networks. These abnormal increased FC patterns are associated with lower cognitive performance which suggest a maladaptive compensatory mechanism in the MCI stage [70, 71]. Similarly, higher nodal topological

properties such as the nodal strength, nodal global efficiency and nodal local efficiency, and increased local and medium-range connectivity located in the DMN-related brain regions were also shown in the earlier subjective cognitive decline stage of AD relative to healthy controls [72]. While these evidence supports our hypothesis of a metabolic compensatory mechanism in the late CN/MCI stage of AD, our findings will need to be confirmed in a larger cohort with longitudinal follow up.

Modest influence of hippocampal structural network deterioration on memory impairment in individuals with non-amyloid pathology

The strength of the association between HIP structural network covariance and memory function was overall lower in non-AD groups compared to amyloid pathology group, which suggested that the hippocampal network integrity had a more modest influence on memory in individuals without Aβ pathology compared to those with Aβ pathology. In line with our finding, a recent study on 531 deceased older community adults showed that neuropathologies such as AD, cerebrovascular disease and hippocampal sclerosis accounted for 42.6% of the variation in global cognitive decline, whereas hippocampal volume alone only accounted for an additional 5.4% of this variation [73]. Furthermore, we demonstrated a non-linear and opposing trajectory of this association as the cognitive stage progresses in non-AD groups compared to AD group. Although prior studies have consistently demonstrated that hippocampal atrophy is associated with memory deficits even before the presence of dementia and can predict dementia progression [74], emerging evidence suggests that the relationship between hippocampal atrophy and memory is also dependent on other factors such as age and cognitive reserve [75, 76, 77]. Specifically, the association between episodic-memory decline and atrophy in the hippocampus over time was stronger in older

than in the middle-aged participants [75]. In middle age, hippocampal volume was related to memory in those with low cognitive reserve, but not in those with high cognitive reserve [76]. Excitingly, our findings shed new insights that the associations of memory decline with both hippocampal structural network integrity and years of education (i.e. a proxy for cognitive reserve) were also dependent on the presence/absence of amyloid pathology and the level of cognitive impairment.

Strengths and Limitations

The main strength of the present study is the inclusion of individuals from the ADNI cohort with well characterized neuropsychological, multimodal neuroimaging and AD biomarker data. This enables the study of the relationships between metabolic, structural brain networks and memory performance specifically in individuals within the AD continuum and those without amyloid pathology. Nevertheless, there are a few limitations in our study. First, the ADNI cohort consists of self-selected individuals participating in a study focusing on AD research which may introduce selection bias and limit the generalizability of our findings to a broader community. Second, our study design is cross-sectional thus provides only indirect evidence on the underlying brain-behavior relationship. Therefore, a larger population-based longitudinal study is needed to characterize within-subject trajectories of brain-behavior relationships across the disease continuum. Lastly, while we characterised the amyloid and tau status of our cohort using CSF amyloid and p-tau, we did not consider the spatial patterns of amyloid and tau brain deposition. Further studies are needed to elucidate the complex spatial and temporal trajectories of structural and metabolic networks in the various non-amyloid tauopathies and how the presence of amyloid affects the tau-metabolism-memory associations across the disease continuum.

In conclusion, our findings support the AD hypothetical models that the association between neurodegeneration and memory dysfunction is non-linear across cognitive stages and depends on the type of pathology. The early influence of metabolic and structural covariance breakdown in the default mode and hippocampal networks on memory performance underscore the importance of early intervention in preclinical AD.

METHODS

Participants

Data used in this article were obtained from the ADNI database (adni.loni.usc.edu). The ADNI was launched in 2003 as a public-private partnership, led by Principal Investigator Michael W. Weiner, MD. The primary goal of ADNI has been to test whether serial MRI, PET, other biological markers, and clinical and neuropsychological assessment can be combined to measure the progression of MCI and early AD.

In this study, we first selected 812 participants to define seed regions for brain network derivation (Figure 1, step 1). All of the images passed the visual quality control. Among them, 232 were CN, 413 were MCI and 167 were probable AD. We then identified 708 participants (610 from ADNI-2 and 98 from ADNI-GO) from the above cohort who underwent neuropsychological assessments, and lumbar puncture in addition to [18F]FDG PET and 3T T1-weighted MRI scans to form the main study cohort (Figure 1, steps 2 & 3). Among them, 195 were CN, 374 were MCI and 139 were probable AD (Table 1). Another larger validation dataset was created for replication by including another 468 individuals (377 from ADNI-1, 38 from ADNI-2, and 53 from ADNI-GO) who underwent 1.5T T1-weighted MRI scan. Supplementary Figure 1 showed the flowchart of study participant selection.

Following ADNI diagnostic criteria [78], we defined CN as those with mini-mental state examination (MMSE) scores ≥ 24 and clinical dementia rating (CDR) 0, and showed no signs of depression, mild cognitive impairment, or dementia. MCI was defined as those with MMSE scores ≥ 24 and CDR 0.5, subjective and objective memory loss, absence of significant levels of impairment in other cognitive domains, essentially preserved activities of daily living, and an absence of dementia. Probable AD was defined as those with MMSE scores ≤ 26, CDR ≥ 0.5 and meeting the NINCDS/ADRDA criteria for probable AD.

Aβ (A) and tau (T) pathologies were measured using CSF $A\beta_{1-42}$ and CSF p-tau_{181p}. More details were in Supplementary Methods. Using the ADNI published cutoffs of $A\beta_{1-42}$ <192 pg/mL and CSF p-tau_{181p} >23 pg/mL to define the presence of Aβ and tau pathology respectively [79], the main study cohort was further stratified into three pathology groups: A-T- (non-amyloid/non-tau), A-T+ (tau only) and A+T-/A+T+ (amyloid pathology) (Table 1). There was no significant difference in age, gender, years of education, and *APOE* ε4 status among CN, MCI, and probable AD individuals in the A-T- and A-T+ groups (Table 1). The proportion of *APOE* ε4 carriers was lower in CN compared to MCI and dementia individuals in the A+T-/A+T+ group.

The ADNI study was approved by the Institutional Review Boards of all of the participating institutions and informed written consent was obtained from all participants at each site.

Neuropsychological assessment

The ADNI-mem is a validated composite memory score derived using data from the ADNI neuropsychological battery [80]. More details were in Supplementary Methods.

Image acquisition and preprocessing

All participants from the main dataset underwent T1-weighted MRI scans according to the standardized ADNI protocol using 3-Tesla scanners. Additional participants who underwent structural MRI brain scans using 1.5-Tesla scanners were included to form a validation dataset with a larger sample size. All participants also underwent [^{18}F]FDG PET to study cerebral glucose metabolism (185 MBq (5 mCi), dynamic 3D scan of six 5-min frames 30-60 min post-injection).

All T1-weighted MRI scans were corrected for field distortions and processed using the CIVET image processing pipeline (www.bic.mni.mcgill.ca/ServicesSoftware/CIVET) to generate the GM probability maps as previously described [81]. [^{18}F]FDG PET images were processed with an in-house processing pipeline as described in our previous work [82]. Further details on image parameters and preprocessing were in Supplementary Methods.

Statistical analyses

Between-group differences in demographic characteristics and clinical assessments were tested among CN, MCI, and probable AD groups. Either a one-way ANOVA or a chi-squared test was used depending on the nature of the variable.

Seed definition: group comparison on GMV and glucose metabolic pattern between CN and probable AD

As shown in Fig. 1 (step 1), the 12 seed coordinates from the DMN, the salience network, the ECN and the memory network were determined based on the group comparisons of the GMV probability and glucose metabolic spatial maps between CN and probable AD individuals using a permutation test (randomise, FSL, 5000 permutations). Effects of age, gender, years of education,

and APOE ε4 genotype were regressed out. The field strength (i.e., 1.5T or 3T) was included as an additional covariate when the tests were performed using the validation dataset (Supplementary Table 1). The resulting GMV and metabolic group difference maps (i.e., CN greater than probable AD) were thresholded using threshold-free cluster enhancement with an alpha level of 0.05 (corrected at family-wise error (FWE) rate). We superimposed the two thresholded t statistical maps (GMV and metabolic) and summed the t-scores at each voxel. Spherical seeds (with 4 mm radius) were then defined based on the peak foci of the above network key regions showing atrophy and hypometabolism in probable AD compared to CN (Supplementary Table 3).

Brain metabolic and structural network derivation: seed PLS analyses

We used seed PLS to identify covariance patterns between GMV/metabolism in each seed region and those of all other voxels in the whole brain (Fig. 1, step 2). The seed value was defined as the average GMV/metabolism values within each predefined seed from step 1. For each seed region, the vector **Y** representing the seed values concatenated across all the participants was cross-correlated with a matrix **X,** representing the GMV (or metabolism) images of all the participants. Both the seed vector **Y** and the image matrix **X** were centered and normalized such that the vector of correlations **R** was computed as:

$$\mathbf{R} = \mathbf{Y}^{\mathbf{T}} \cdot \mathbf{X}.$$

Using singular value decomposition, the correlation vector **R** was decomposed into a set of mutually orthogonal latent variables (LVs) comprising three matrices:

$$\mathbf{R} = \mathbf{v} \cdot \mathbf{s} \cdot \mathbf{u}^{\mathbf{T}},$$

where **s** is the diagonal matrix of singular values, and **v** and **u** are the orthonormal matrices of left and right singular vectors, which are also called saliences in the PLS terminology. The left and

right singular vectors respectively represent the seed profiles and the whole-brain patterns that best characterize the correlation vector **R**. Therefore, the brain salience **u** captures the brain covariance or network pattern that is of interest. The number of LVs derived is equal to the rank of the correlations vector **R**. The LVs were tested for statistical significance with 1000 permutations. The stability of each voxel in the brain salience of the LV was validated using a bootstrap ratio, calculated by dividing the voxel salience value by its standard error, estimated by bootstrapping (500 times).

The resulting significant LV from the PLS analyses of each of the 12 seeds (all $p < 0.0001$) corresponded to reliable patterns of structural or metabolic covariance network associated with that seed (see Supplementary Fig. 2).

To represent individual-level brain salience maps of the identified LV for each seed PLS model, the original matrix **X** was projected onto the brain salience **u**, which was computed by:

$$\mathbf{L_X} = \mathbf{X} \cdot \mathbf{u},$$

where $\mathbf{L_X}$ is a vector of brain structural or metabolic network scores across all the participants.

We calculated the brain network score for each of the 12 networks in both FDG and GMV modalities separately. For HIP, ANG, INS, PPC, and DLPFC, we averaged the left and right brain network scores. In total, each participant had 14 brain network scores (i.e., two for each of the 7 seed regions, including HIP, ANG, PCC, mPFC, INS, PPC, and DLPFC), which reflect structural or metabolic network pattern expression.

Stage- and pathology-dependent associations between brain networks and memory impairment: SVC modelling

With ADNI-mem as the dependent variable, the SVC models have the following form:

$$y_i(t_k) = \sum_{j=1}^{p} \beta_j(t_k) x_{ij}(t_k) + \varepsilon_i(t_k),$$

where the dependent variable $y_i(t_k)$ represents the cognitive score for subject i ($i = 1, 2, \ldots, n$) at the bin t_k ($k = 1, 2, \ldots, K$), $x_{ij}(t_k)$ is the j^{th} ($j = 1, 2, \ldots, p$) predictor (FDG/GMV network scores and nuisance variables; see below) of subject i at the bin t_k. Both the dependent variable and all predictors were standardized to z-scores. $\beta_j(t_k)$ is the coefficient function depending on bin t_k for each feature j and $\varepsilon_i(t_k)$ is the independent and identically distributed random errors at t_k. The coefficient function $\beta_j(t_k)$ is approximated using linear combinations of a set of B-spline basis. To simultaneously achieve regression model fitting and variable selection, the least absolute shrinkage and selection operator (LASSO) [83] is applied to estimate $\beta_j(t_k)$ by minimizing the following penalized least squares function:

$$\frac{1}{2n} \sum_{i=1}^{n} \sum_{k=1}^{K} [y_i(t_k) - \sum_{j=1}^{p} \beta_j(t_k) x_{ij}(t_k)]^2 + \lambda \sum_{j=1}^{p} \sqrt{\int \beta_j^2(t) dt},$$

where λ is the sparse penalty tuning parameter, which was chosen by a five-fold cross-validation method.

We ran each SVC model for 100 repetitions and reported the brain measures that were consistently selected by more than 90 repetitions. These measures were interpreted as a set of critical brain GMV/metabolism networks that contributed to memory across the cognitive stages, with a vector of beta coefficients reflecting stage-dependent (non)linearity in the network-memory association.

To assess the stability of these beta coefficients, we calculated the mean and standard error of the stage/pathology-dependent coefficients estimated from all 100 repetitions. Moreover, to assess the specificity of the selected networks, we randomly permuted the memory scores 100 times across the participants and repeated the SVC modelling 100 times within each of the 100

permuted data sets, following our previous approach [45]. These 'null' permutations should yield inconsistent selection of predictors, if any, as compared to our actual models. SVC modelling was performed by in-house R scripts based on Daye and colleagues [46].

To further confirm that our findings were robust, we repeated the analyses with another ordering strategy which did not divide MCI and probable AD into two separate groups (i.e., CDR-SOB and age ordering were done across all individuals with either MCI or probable AD diagnosis) in each pathology group (Supplementary Fig. 4B).

To compare the brain metabolic and structural network scores between different cognitive stages and differenct pathology groups (Fig. 1, step 3), we performed ANOVA among the cognitive stages for each pathology, and ANOVA among the pathology groups for each cognitive stage, followed by post-hoc two-sample t-tests (alpha = 0.05).

DISCLOSURE STATEMENT

The authors have no potential conflicts of interest.

ACKNOWLEDGEMENTS

Data collection and sharing for this project was funded by the Alzheimer's Disease Neuroimaging Initiative (ADNI) (National Institutes of Health Grant U01 AG024904) and DOD ADNI (Department of Defense award number W81XWH-12-2-0012). ADNI is funded by the National Institute on Aging, the National Institute of Biomedical Imaging and Bioengineering, and through generous contributions from the following: AbbVie, Alzheimer's Association; Alzheimer's Drug Discovery Foundation; Araclon Biotech; BioClinica, Inc.; Biogen; Bristol-Myers Squibb Company; CereSpir, Inc.; Cogstate; Eisai Inc.; Elan Pharmaceuticals, Inc.; Eli Lilly and Company;

EuroImmun; F. Hoffmann-La Roche Ltd and its affiliated company Genentech, Inc.; Fujirebio; GE Healthcare; IXICO Ltd.; Janssen Alzheimer Immunotherapy Research & Development, LLC.; Johnson & Johnson Pharmaceutical Research & Development LLC.; Lumosity; Lundbeck; Merck & Co., Inc.; Meso Scale Diagnostics, LLC.; NeuroRx Research; Neurotrack Technologies; Novartis Pharmaceuticals Corporation; Pfizer Inc.; Piramal Imaging; Servier; Takeda Pharmaceutical Company; and Transition Therapeutics. The Canadian Institutes of Health Research is providing funds to support ADNI clinical sites in Canada. Private sector contributions are facilitated by the Foundation for the National Institutes of Health (www.fnih.org). The grantee organization is the Northern California Institute for Research and Education, and the study is coordinated by the Alzheimer's Therapeutic Research Institute at the University of Southern California. ADNI data are disseminated by the Laboratory for Neuro Imaging at the University of Southern California. We also acknowledge the funding support from Yong Loo Lin School of Medicine, National University of Singapore (J.H.Z), the Duke-NUS/Khoo Bridge Funding Award (J.H.Z., KBrFA/2019-0020), NMRC Open Fund Large Collaborative Grant (J.H.Z., OFLCG09May0035).

AUTHOR CONTRIBUTIONS

Kok Pin Ng: conception and design of the study, data analysis, results interpretation, drafting the manuscript and figures

Xing Qian: conception and design of the study, data analysis, results interpretation, drafting the manuscript and figures

Kwun Kei Ng: manuscript revision and scripting

Fang Ji: manuscript revision and scripting

Pedro Rosa-Neto: reviewing the manuscript

Serge Gauthier: reviewing the manuscript

Nagaendran Kandiah: reviewing the manuscript

Juan Helen Zhou: conception and design of the study, results interpretation, drafting and critical review of the manuscript

MATERIALS & CORRESPONDENCE

Requests for data and code can be addressed to the Corresponding Author, Juan Helen Zhou.

REFERENCES

1. Braak H, Braak E. Neuropathological stageing of Alzheimer-related changes. *Acta neuropathologica* **82**, 239-259 (1991).

2. Serrano-Pozo A, Frosch MP, Masliah E, Hyman BT. Neuropathological alterations in Alzheimer disease. *Cold Spring Harbor perspectives in medicine* **1**, a006189 (2011).

3. Jack CR, *et al*. A/T/N: an unbiased descriptive classification scheme for Alzheimer disease biomarkers. *Neurology* **87**, 539-547 (2016).

4. Jack Jr CR, *et al*. NIA-AA research framework: toward a biological definition of Alzheimer's disease. *Alzheimer's & Dementia* **14**, 535-562 (2018).

5. Knopman DS, *et al*. The National Institute on Aging and the Alzheimer's Association Research Framework for Alzheimer's disease: perspectives from the research roundtable. *Alzheimer's & Dementia* **14**, 563-575 (2018).

6. Bateman RJ, *et al*. Clinical and biomarker changes in dominantly inherited Alzheimer's disease. *N Engl J Med* **367**, 795-804 (2012).

7. Jack Jr CR, *et al*. Tracking pathophysiological processes in Alzheimer's disease: an updated hypothetical model of dynamic biomarkers. *The Lancet Neurology* **12**, 207-216 (2013).

8. Bertens D, Knol DL, Scheltens P, Visser PJ, Initiative AsDN. Temporal evolution of biomarkers and cognitive markers in the asymptomatic, MCI, and dementia stage of Alzheimer's disease. *Alzheimer's & Dementia* **11**, 511-522 (2015).

9. Chételat G, *et al*. Direct voxel-based comparison between grey matter hypometabolism and atrophy in Alzheimer's disease. *Brain* **131**, 60-71 (2008).

10. Misra C, Fan Y, Davatzikos C. Baseline and longitudinal patterns of brain atrophy in MCI patients, and their use in prediction of short-term conversion to AD: results from ADNI. *Neuroimage* **44**, 1415-1422 (2009).

11. Mosconi L, *et al*. FDG-PET changes in brain glucose metabolism from normal cognition to pathologically verified Alzheimer's disease. *European journal of nuclear medicine and molecular imaging* **36**, 811-822 (2009).

12. Kljajevic V, Grothe MJ, Ewers M, Teipel S, Initiative AsDN. Distinct pattern of hypometabolism and atrophy in preclinical and predementia Alzheimer's disease. *Neurobiology of aging* **35**, 1973-1981 (2014).

13. Hanseeuw BJ, *et al*. Fluorodeoxyglucose metabolism associated with tau-amyloid interaction predicts memory decline. *Annals of neurology* **81**, 583-596 (2017).

14. Pascoal TA, *et al*. Amyloid-β and hyperphosphorylated tau synergy drives metabolic decline in preclinical Alzheimer's disease. *Molecular psychiatry* **22**, 306-311 (2017).

15. Jack CR, *et al*. Amyloid-first and neurodegeneration-first profiles characterize incident amyloid PET positivity. *Neurology* **81**, 1732-1740 (2013).

16. Ballatore C, Lee VM-Y, Trojanowski JQ. Tau-mediated neurodegeneration in Alzheimer's disease and related disorders. *Nature reviews neuroscience* **8**, 663-672 (2007).

17. Zhou J, Gennatas ED, Kramer JH, Miller BL, Seeley WW. Predicting regional neurodegeneration from the healthy brain functional connectome. *Neuron* **73**, 1216-1227 (2012).

18. Seeley WW, Crawford RK, Zhou J, Miller BL, Greicius MD. Neurodegenerative diseases target large-scale human brain networks. *Neuron* **62**, 42-52 (2009).

19. Marchitelli R, *et al*. Simultaneous resting-state FDG-PET/fMRI in Alzheimer disease: relationship between glucose metabolism and intrinsic activity. *Neuroimage* **176**, 246-258 (2018).

20. Greicius MD, Srivastava G, Reiss AL, Menon V. Default-mode network activity distinguishes Alzheimer's disease from healthy aging: evidence from functional MRI. *Proceedings of the National Academy of Sciences* **101**, 4637-4642 (2004).

21. Zhou J, *et al*. Divergent network connectivity changes in behavioural variant frontotemporal dementia and Alzheimer's disease. *Brain* **133**, 1352-1367 (2010).

22. Chong JSX, *et al*. Influence of cerebrovascular disease on brain networks in prodromal and clinical Alzheimer's disease. *Brain* **140**, 3012-3022 (2017).

23. Chong JSX, *et al*. Amyloid and cerebrovascular burden divergently influence brain functional network changes over time. *Neurology* **93**, e1514-e1525 (2019).

24. Zhou J, Liu S, Ng KK, Wang J. Applications of resting-state functional connectivity to neurodegenerative disease. *Neuroimaging Clinics* **27**, 663-683 (2017).

25. Brier MR, *et al*. Loss of intranetwork and internetwork resting state functional connections with Alzheimer's disease progression. *Journal of Neuroscience* **32**, 8890-8899 (2012).

26. He X, *et al*. Abnormal salience network in normal aging and in amnestic mild cognitive impairment and Alzheimer's disease. *Human brain mapping* **35**, 3446-3464 (2014).

27. Ripp I, *et al*. Integrity of Neurocognitive Networks in Dementing Disorders as Measured with Simultaneous PET/Functional MRI. *Journal of Nuclear Medicine* **61**, 1341-1347 (2020).

28. Zielinski BA, Gennatas ED, Zhou J, Seeley WW. Network-level structural covariance in the developing brain. *Proceedings of the National Academy of Sciences* **107**, 18191-18196 (2010).

29. Montembeault M, *et al*. The impact of aging on gray matter structural covariance networks. *Neuroimage* **63**, 754-759 (2012).

30. Lizarraga A, Ripp I, Yakushev I. Relationships between MRI-and PET-based measures of brain connectivity. (ed^(eds). Soc Nuclear Med (2021).

31. Li K, *et al*. Gray matter structural covariance networks changes along the Alzheimer's disease continuum. *NeuroImage: Clinical* **23**, 101828 (2019).

32. Kim H-J, *et al*. Using individualized brain network for analyzing structural covariance of the cerebral cortex in Alzheimer's patients. *Frontiers in neuroscience* **10**, 394 (2016).

33. Tijms BM, Seriès P, Willshaw DJ, Lawrie SM. Similarity-based extraction of individual networks from gray matter MRI scans. *Cerebral cortex* **22**, 1530-1541 (2012).

34. Tijms BM, *et al*. Gray matter networks and clinical progression in subjects with predementia Alzheimer's disease. *Neurobiology of aging* **61**, 75-81 (2018).

35. Tijms BM, *et al*. Single-subject gray matter graph properties and their relationship with cognitive impairment in early-and late-onset Alzheimer's disease. *Brain connectivity* **4**, 337-346 (2014).

36. Vermunt L, *et al*. Single-subject grey matter network trajectories over the disease course of autosomal dominant Alzheimer's disease. *Brain communications* **2**, fcaa102 (2020).

37. Tijms BM, *et al*. Single-subject grey matter graphs in Alzheimer's disease. *PloS one* **8**, e58921 (2013).

38. Liu Z, *et al*. Resolving heterogeneity in schizophrenia through a novel systems approach to brain structure: individualized structural covariance network analysis. *Molecular Psychiatry*, 1-13 (2021).

39. Habeck C, *et al*. Relationship between baseline brain metabolism measured using [18 F] FDG PET and memory and executive function in prodromal and early Alzheimer's disease. *Brain imaging and behavior* **6**, 568-583 (2012).

40. Bejanin A, *et al*. Tau pathology and neurodegeneration contribute to cognitive impairment in Alzheimer's disease. *Brain* **140**, 3286-3300 (2017).

41. Sabuncu MR, *et al*. The dynamics of cortical and hippocampal atrophy in Alzheimer disease. *Archives of neurology* **68**, 1040-1048 (2011).

42. Schuff N, *et al*. Nonlinear time course of brain volume loss in cognitively normal and impaired elders. *Neurobiology of aging* **33**, 845-855 (2012).

43. Caroli A, Frisoni G, Initiative AsDN. The dynamics of Alzheimer's disease biomarkers in the Alzheimer's Disease Neuroimaging Initiative cohort. *Neurobiology of aging* **31**, 1263-1274 (2010).

44. Krishnan A, Williams LJ, McIntosh AR, Abdi H. Partial Least Squares (PLS) methods for neuroimaging: a tutorial and review. *Neuroimage* **56**, 455-475 (2011).

45. Hong Z, *et al*. Differential age-dependent associations of gray matter volume and white matter integrity with processing speed in healthy older adults. *Neuroimage* **123**, 42-50 (2015).

46. Daye ZJ, Xie J, Li H. A sparse structured shrinkage estimator for nonparametric varying-coefficient model with an application in genomics. *Journal of Computational and Graphical Statistics* **21**, 110-133 (2012).

47. Ji F, *et al*. White matter microstructural abnormalities and default network degeneration are associated with early memory deficit in Alzheimer's disease continuum. *Scientific reports* **9**, 1-11 (2019).

48. Zhang L, *et al*. Longitudinal trajectory of Amyloid-related hippocampal subfield atrophy in nondemented elderly. *Human brain mapping* **41**, 2037-2047 (2020).

49. Veldsman M, *et al*. Degeneration of structural brain networks is associated with cognitive decline after ischaemic stroke. *Brain communications* **2**, fcaa155 (2020).

50. Vincent JL, Kahn I, Snyder AZ, Raichle ME, Buckner RL. Evidence for a frontoparietal control system revealed by intrinsic functional connectivity. *Journal of neurophysiology* **100**, 3328-3342 (2008).

51. Tulving E, Markowitsch HJ. Episodic and declarative memory: role of the hippocampus. *Hippocampus* **8**, 198-204 (1998).

52. Eichenbaum H. Hippocampus: cognitive processes and neural representations that underlie declarative memory. *Neuron* **44**, 109-120 (2004).

53. Coupé P, Manjón JV, Lanuza E, Catheline G. Lifespan changes of the human brain in Alzheimer's disease. *Scientific reports* **9**, 1-12 (2019).

54. Bayram E, Caldwell JZ, Banks SJ. Current understanding of magnetic resonance imaging biomarkers and memory in Alzheimer's disease. *Alzheimer's & Dementia: Translational Research & Clinical Interventions* **4**, 395-413 (2018).

55. Wang L, *et al*. Spatially distinct atrophy is linked to β-amyloid and tau in preclinical Alzheimer disease. *Neurology* **84**, 1254-1260 (2015).

56. Mormino E, *et al*. Episodic memory loss is related to hippocampal-mediated β-amyloid deposition in elderly subjects. *Brain* **132**, 1310-1323 (2009).

57. Lim YY, *et al*. Relationships between performance on the Cogstate Brief Battery, neurodegeneration, and Aβ accumulation in cognitively normal older adults and adults with MCI. *Archives of Clinical Neuropsychology* **30**, 49-58 (2015).

58. Mattsson N, *et al*. Brain structure and function as mediators of the effects of amyloid on memory. *Neurology* **84**, 1136-1144 (2015).

59. Treves A, Rolls ET. Computational analysis of the role of the hippocampus in memory. *Hippocampus* **4**, 374-391 (1994).

60. Blumenfeld RS, Ranganath C. Prefrontal cortex and long-term memory encoding: an integrative review of findings from neuropsychology and neuroimaging. *The Neuroscientist* **13**, 280-291 (2007).

61. Doré V, *et al*. Cross-sectional and longitudinal analysis of the relationship between Aβ deposition, cortical thickness, and memory in cognitively unimpaired individuals and in Alzheimer disease. *JAMA neurology* **70**, 903-911 (2013).

62. Defrancesco M, *et al*. Changes in white matter integrity before conversion from mild cognitive impairment to Alzheimer's disease. *PloS one* **9**, e106062 (2014).

63. Jeong H, Park J, Song I, Chung Y, Rhie S. Changes in cognitive function and brain glucose metabolism in elderly women with subjective memory impairment: a 24-month prospective pilot study. *Acta Neurologica Scandinavica* **135**, 108-114 (2017).

64. Hammond TC, *et al*. β-amyloid and tau drive early Alzheimer's disease decline while glucose hypometabolism drives late decline. *Communications biology* **3**, 1-13 (2020).

65. Tomasi D, Volkow ND. Functional connectivity hubs in the human brain. *Neuroimage* **57**, 908-917 (2011).

66. Jonides J, *et al*. The role of parietal cortex in verbal working memory. *Journal of neuroscience* **18**, 5026-5034 (1998).

67. Seghier ML. The angular gyrus: multiple functions and multiple subdivisions. *The Neuroscientist* **19**, 43-61 (2013).

68. Ciaramelli E, Grady CL, Moscovitch M. Top-down and bottom-up attention to memory: a hypothesis (AtoM) on the role of the posterior parietal cortex in memory retrieval. *Neuropsychologia* **46**, 1828-1851 (2008).

69. Pascoal TA, *et al*. Aβ-induced vulnerability propagates via the brain's default mode network. *Nature communications* **10**, 1-13 (2019).

70. Gardini S, *et al*. Increased functional connectivity in the default mode network in mild cognitive impairment: a maladaptive compensatory mechanism associated with poor semantic memory performance. *Journal of Alzheimer's Disease* **45**, 457-470 (2015).

71. Liang J, *et al*. Increased intrinsic default-mode network activity as a compensatory mechanism in aMCI: a resting-state functional connectivity MRI study. *Aging (Albany NY)* **12**, 5907 (2020).

72. Chen H, *et al*. The compensatory phenomenon of the functional connectome related to pathological biomarkers in individuals with subjective cognitive decline. *Translational neurodegeneration* **9**, 1-14 (2020).

73. Dawe RJ, Yu L, Arfanakis K, Schneider JA, Bennett DA, Boyle PA. Late-life cognitive decline is associated with hippocampal volume, above and beyond its associations with traditional neuropathologic indices. *Alzheimer's & Dementia* **16**, 209-218 (2020).

74. Ferrarini L, *et al*. Hippocampal atrophy in people with memory deficits: results from the population-based IPREA study. *International psychogeriatrics* **26**, 1067-1081 (2014).

75. Gorbach T, *et al*. Longitudinal association between hippocampus atrophy and episodic-memory decline. *Neurobiology of aging* **51**, 167-176 (2017).

76. Vuoksimaa E, *et al*. Cognitive reserve moderates the association between hippocampal volume and episodic memory in middle age. *Neuropsychologia* **51**, 1124-1131 (2013).

77. Svenningsson AL, Stomrud E, Insel PS, Mattsson N, Palmqvist S, Hansson O. β-amyloid pathology and hippocampal atrophy are independently associated with memory function in cognitively healthy elderly. *Scientific reports* **9**, 1-9 (2019).

78. Petersen RC, *et al*. Alzheimer's disease neuroimaging initiative (ADNI): clinical characterization. *Neurology* **74**, 201-209 (2010).

79. Shaw LM, *et al*. Cerebrospinal fluid biomarker signature in Alzheimer's disease neuroimaging initiative subjects. *Annals of neurology* **65**, 403-413 (2009).

80. Crane PK, *et al*. Development and assessment of a composite score for memory in the Alzheimer's Disease Neuroimaging Initiative (ADNI). *Brain imaging and behavior* **6**, 502-516 (2012).

81. Kang MS, *et al*. Amyloid-beta modulates the association between neurofilament light chain and brain atrophy in Alzheimer's disease. *Molecular Psychiatry*, 1-13 (2020).

82. Ng KP, *et al*. Neuropsychiatric symptoms predict hypometabolism in preclinical Alzheimer disease. *Neurology* **88**, 1814-1821 (2017).

83. Tibshirani R. Regression shrinkage and selection via the lasso. *Journal of the Royal Statistical Society: Series B (Methodological)* **58**, 267-288 (1996).

SUPPLEMENTARY METHODS

CSF analysis

CSF AD biomarkers of $A\beta_{1-42}$ and CSF p-tau_{181p} were measured using the Luminex multiplex platform (Luminex, Austin, TX, USA) and Innogenetics INNO-BIA AlzBio3 (Innogenetics, Ghent, Belgium) immunoassay reagents. The details of the ADNI methods for the acquisition and measurement of CSF can be found at www.adni-info.org.

Neuropsychological assessment

The ADNI-mem is a validated composite memory score derived using data from the ADNI neuropsychological battery [1]. A modern psychometric approach was used to analyze the Rey Auditory Verbal Learning Test, AD assessment schedule-cognition (ADAS-cog), MMSE, and Logical Memory tests to obtain a composite memory score. In ADNI-mem composite scores, lower scores reflect poorer memory performance. The details of the ADNI protocols for the neuropsychological assessments and the methods for developing the ADNI-mem can be found at www.adni-info.org.

Image acquisition and preprocessing

All participants from the main dataset underwent T1-weighted MRI scans according to the standardized ADNI protocol using 3-Tesla GE, Philips, and Siemens MRI scanners with a sagittal volumetric magnetization-prepare rapid-acquisition gradient echo (MPRAGE) sequence (TR=2300ms, TE = minimum full, approximate TI=900ms, Slice Thickness=1.2, flip-angle = 9°) or T1-weighted accelerated sagittal inversion-recovery spoiled gradient-recalled (SPGR) sequence (TR = 400 ms, TE = minimum full, flip-angle = 11°, slice thickness = 1.2 mm and FOV = 26 cm).

Additional participants who underwent structural MRI brain scans using 1.5-tesla GE, Philips, and Siemens MRI scanners were included to form a validation dataset with a larger sample size. For these participants, T1-weighted MRI scans were acquired using an MPRAGE sequence with TR=2400ms, minimum full TE, TI=1000ms, Slice Thickness=1.2, and flip angle of 8 degrees (scan parameters vary between sites, scanner platforms, and software versions).

All participants also underwent [^{18}F]FDG PET to study cerebral glucose metabolism (185 MBq (5 mCi), dynamic 3D scan of six 5-min frames 30-60 min post-injection). Further details on MRI and PET acquisition parameters can be found at the ADNI website http://adni.loni.usc.edu/methods.

Voxel-based morphometry

All T1-weighted MRI scans were corrected for field distortions and processed using the CIVET image processing pipeline (www.bic.mni.mcgill.ca/ServicesSoftware/CIVET). The MRI images underwent non-uniformity correction, brain masking and segmentation, and normalization to the Montreal Neurological Institute (MNI) space with affine and nonlinear transformation. An in-house processing pipeline based on MINC toolkits was then applied to generate voxel-based morphometry (VBM) images based on the CIVET outputs as previously described [2]. In brief, a log Jacobian determinant was derived based on the nonlinear vector field from the CIVET outputs, followed by transformation into a scalar, modulated with grey matter probability mask. The GM probability maps were then smoothed with an 8mm Full-Width at Half-Maximum (FWHM) Gaussian kernel.

[^{18}F]FDG PET processing

[^{18}F]FDG PET images were processed with an in-house processing pipeline as described in our previous work [3]. The pre-processed images from the ADNI database were smoothed with an 8mm FWHM Gaussian kernel, followed by linear co-registration and non-linear spatial normalization to the MNI 152 standardized space with the use of transformation matrices derived from the PET native to MRI native space and the MRI native to the MNI 152 space. The voxel-wise brain glucose metabolism standardized uptake value ratio (SUVR) maps were then generated with the pons as the reference region.

SUPPLEMENTARY RESULTS

The ANG-based metabolic and HIP-based structural network findings were replicated in both the main and validation datasets (Supplementary Fig. 2, 3, and 7). In addition, in the main dataset, lower insular metabolic network score was identified to be associated with lower memory impairment only in the A-T+ group, the influence of which was highest in the early CN stage and gradually decreased across CN and MCI stages before regaining a minimum influence in the late MCI/dementia stages. However, this finding was not replicated in the validation dataset.

References

1. Crane PK, *et al.* Development and assessment of a composite score for memory in the Alzheimer's Disease Neuroimaging Initiative (ADNI). *Brain imaging and behavior* **6**, 502-516 (2012).

2. Kang MS, *et al.* Amyloid-beta modulates the association between neurofilament light chain and brain atrophy in Alzheimer's disease. *Molecular Psychiatry*, 1-13 (2020).

3. Ng KP, *et al.* Neuropsychiatric symptoms predict hypometabolism in preclinical Alzheimer disease. *Neurology* **88**, 1814-1821 (2017).

SUPPLEMENTARY TABLES

Supplementary Table 1. Participants demographics for network seed definition step.

	Main dataset			Validation dataset		
	CN	**probable AD**	**p-value**	**CN**	**probable AD**	**p-value**
N	232	167	-	383	360	-
Age, y	56.53~90.22	55.96~90.50		56.53~93.80	55.33~90.50	
	73.52±6.27	74.35±8.07	0.25	74.90±6.35	75.48±7.62	0.26
Gender (M/F)	110/122	99/68	0.02*	195/188	214/146	0.02*
Handedness (R/L)	207/25	154/13	0.32	346/37	336/24	0.14
Education, y	16.23±2.54	15.95±2.68	0.01*	16.31±2.77	15.66±2.87	0.002*
APOE e4 (+/-)	158/74	53/114	<0.001*	274/108	120/239	<0.001*
Memory	1.07±0.62	-0.82±0.59	<0.001*	1.02±0.60	-0.85±0.61	<0.001*
MMSE	29.01±1.23	23.30±2.37	<0.001*	29.02±1.20	22.83±3.36	<0.001*
CDR-SOB	0.05±0.16	4.59±1.70	<0.001*	0.02±0.47	4.77±2.08	<0.001*

Note: Data on age are range and mean ± SD. Data on education and memory are mean ± SD. Data on memory are in z-scores. Abbreviations: CN = cognitively normal; MCI = mild cognitive impairment; AD = Alzheimer's disease; A= β-amyloid; T = tau; '+' = positive; '-' = negative; y = years; M = male; F = female; R = right; L = left; MMSE = Mini-Mental State Exam; CDR-SOB = Clinical Dementia Rating scale-sum of box. * indicate significant group difference between CN and probable AD.

Supplementary Table 2. Study participant demographics of the validation dataset for the PLS-SVC model.

	A-T-			A-T+			A+T-/A+T+		
	CN	**MCI**	**probable AD**	**CN**	**MCI**	**probable AD**	**CN**	**MCI**	**probable AD**
N	56	82	5	92	79	11	114	264	156
Age, y	62.24~90.13	56.08~88.51	69.56~90.50	56.53~93.80	55.15~88.98	60.79~81.37	60.19~90.08	55.38~91.57	55.96~90.46
	74.0±6.09[m]	70.62±7.53[cd]	79.51±9.22[m]	72.81±6.36[m]	70.54±8.41[cd]	76.22±6.52[m]	75.65±6.33[m]	73.70±6.79[c]	74.24±7.88
Gender (M/F)	29/27	45/37	5/0	52/40[d]	40/39[d]	10/1[cm]	53/61	154/110	89/67
Handedness (R/L)	53/3	68/14	5/0	81/11	71/8	10/1	107/7	240/24	144/12
Education, y	16.23±2.90	16.40±2.58	15.60±4.39	16.71±2.75	16.01±2.69	16.27±2.41	16.27±2.56	16.11±2.75	15.85±2.65
APOE e4 (+/-)	9/47	17/65	0/5	17/75	18/61	1/10	49/65[md]	160/104[cd]	113/43[cm]
Memory	1.06±0.66[md]	0.69±0.64[cd]	-0.35±0.78[cm]	1.12±0.57[md]	0.53±0.62[cd]	-0.54±0.64[cm]	0.95±0.61[md]	0.17±0.63[cd]	-0.88±0.53[cm]

MMSE	28.93±1.44[d]	28.52±1.34[d]	25.40±2.19[cm]	28.96±1.19[md]	28.27±1.65[cd]	24.0±2.05[cm]	29.07±1.15[md]	27.77±1.82[cd]	22.89±2.67[cm]
CDR-SOB	0.05±0.18[md]	1.23±0.64[cd]	4.20±2.66[cm]	0.05±0.15[md]	1.22±0.75[cd]	4.32±1.23[cm]	0.04±0.15[md]	1.52±0.91[cd]	4.73±1.85[cm]
ICV	1564.58± 148.69	1528.79± 131.03	1583.20± 99.88	1554.05± 135.70	1559.29± 145.90	1599.97± 183.02	1536.14± 145.69	1567.10± 148.96.52	1551.78± 161.75

Note: Data on age are range and mean ± SD. Data on education, ICV and memory are mean ± SD. Data on memory are in z-scores. Abbreviations: CN = cognitively normal; MCI = mild cognitive impairment; AD = Alzheimer's disease; A= β-amyloid; T = tau; '+' = positive; '-' = negative; y = years; M = male; F = female; R = right; L = left; MMSE = Mini-Mental State Exam; CDR-SOB = Clinical Dementia Rating scale-sum of box; ICV = intracranial volume. Superscripts ('[c]', '[m]', '[d]') represent significant group difference with CN, MCI and probable AD respectively.

Supplementary Table 3. The coordinates of the peak foci of regions showing difference in metabolism and grey matter volume between probable AD and healthy controls.

		Main dataset			Validation dataset		
Network Label	**Anatomical Label**	**x**	**y**	**z**	**x**	**y**	**z**
Hippocampus	left HIP	-19	-3	-22	-33	-18	-17
	right HIP	19	-3	-21	19	-2	-22
Default mode	left ANG	-47	-63	39	-46	-63	39
	right ANG	50	-60	37	51	-60	37
	PCC	-4	-52	29	-4	-52	27
	mPFC	1	50	-5	-2	57	4
Salience	left INS	-43	0	-10	-43	-4	-5
	right INS	44	-2	-7	44	-2	-5
Executive	left DLPFC	-46	11	40	-46	11	40
control	right DLPFC	42	15	40	42	15	40
	left PPC	-53	-45	43	-52	-46	45
	right PPC	52	-52	44	52	-52	44

Abbreviations: HIP = hippocampus; ANG = angular gyrus; PPC = posterior parietal cortex; mPFC = medial prefrontal cortex; INS = insular; DLPFC = dorsolateral prefrontal cortex; PCC = posterior cingulate cortex.

SUPPLEMENTARY FIGURES

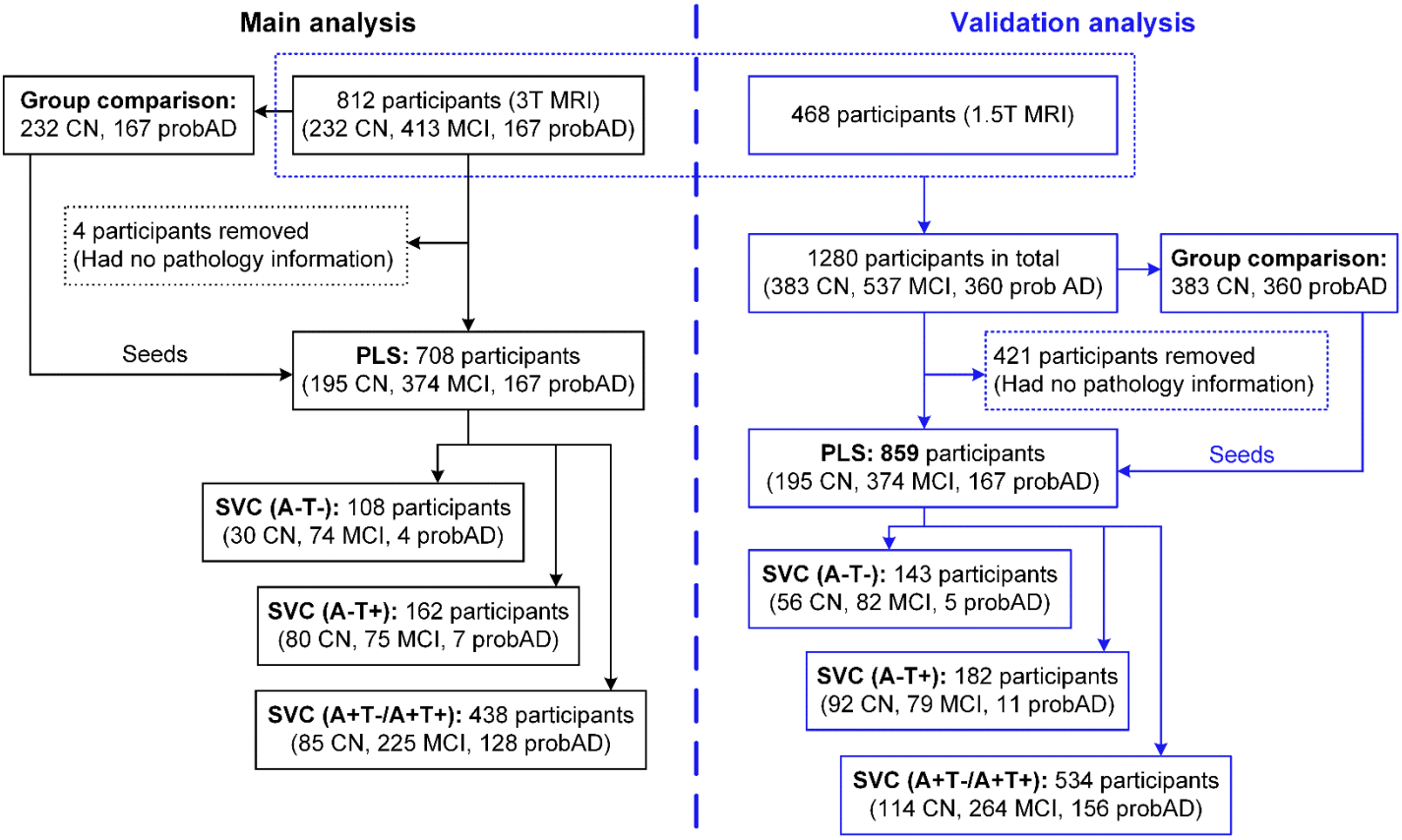

Supplementary Figure 1. Flowchart of participant pool selection. Abbreviations: CN = cognitively normal; MCI = mild cognitive impairment; probAD = probable AD; A= β-amyloid; T = tau; '+' = positive; '-' = negative; PLS = partial least square analysis; SVC = sparse varying coefficient modelling.

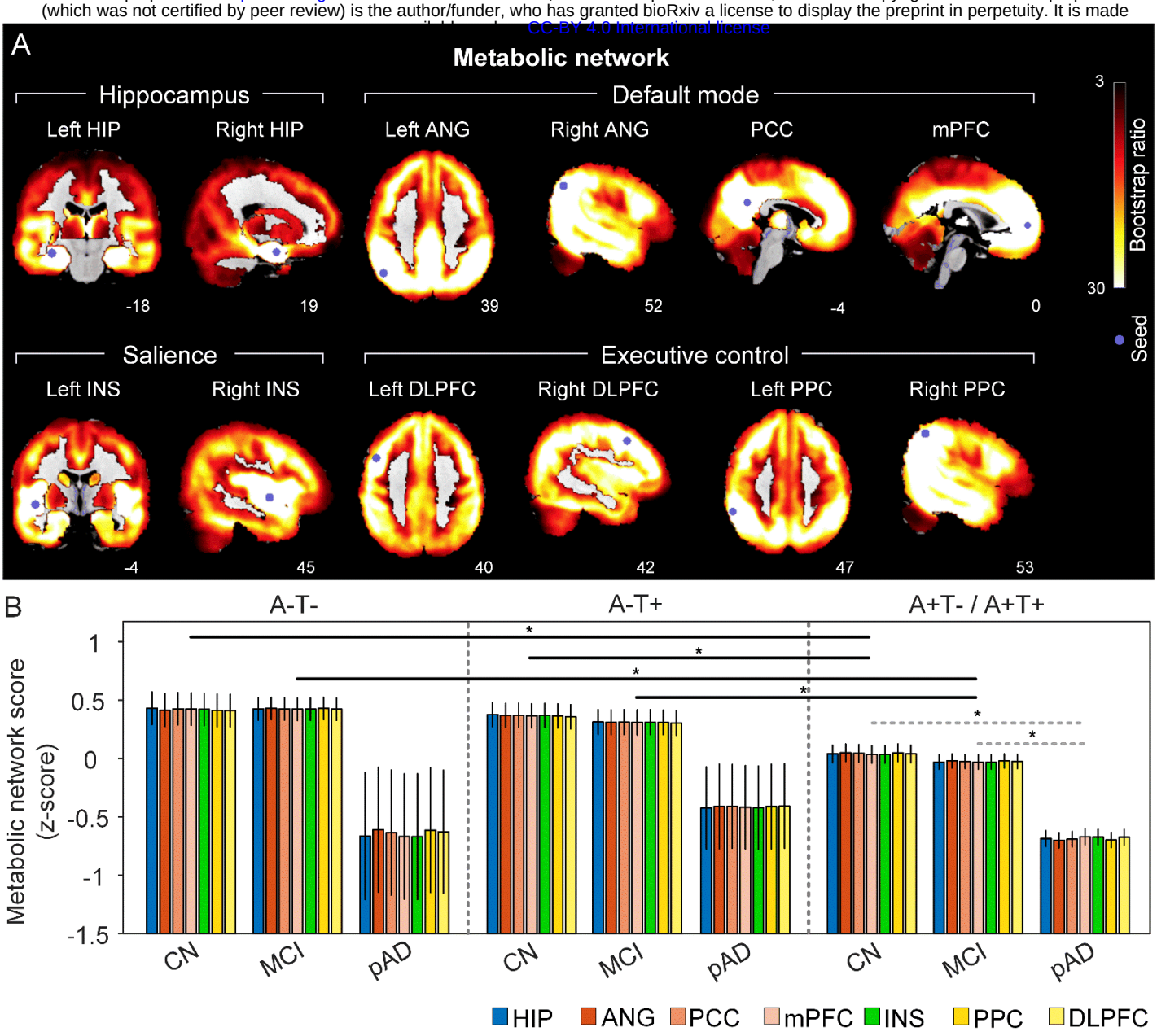

Supplementary Figure 2. The integrity of brain metabolic networks in participants with and without amyloid pathology across cognitive stages (validation dataset). A. Brain slices of metabolic covariance networks associated with each brain seed defined from FDG-PET data highlighted in blue circles. Brain metabolic network resemabled canonical brain networks. The intensity of colorbar represents bootstrap ratios, derived from dividing the weight of the singular-vector by the bootstrapped standard error. **B**. Individual-level brain metabolic network scores were lower in individuals with worse cognition and amyloid pathology. Summary of individual-level metabolic network scores (mean ± SD) were presented in bar charts. '*' indicates significant group difference (ANOVA; $p < 0.05$). Thick lines indicate group differences in brain network scores between different cognitive stages (grey dashed) or pathology groups (dark). Abbreviations: HIP = hippocampus; ANG = angular gyrus; PCC = posterior cingulate cortex; mPFC = media prefrontal cortex; INS = insular; DLPFC = dorsolateral prefrontal cortex; PPC = posterior parietal cortex; CN = cognitively normal; MCI

= mild cognitive impairment; pAD = probable AD; A= β-amyloid; T = tau; '+' = positive; '-' = negative; HIP = hippocampus; ANG = angular gyrus; PCC = posterior cingulate cortex; mPFC = media prefrontal cortex; INS = insular; DLPFC = dorsolateral prefrontal cortex; PPC = posterior parietal cortex.

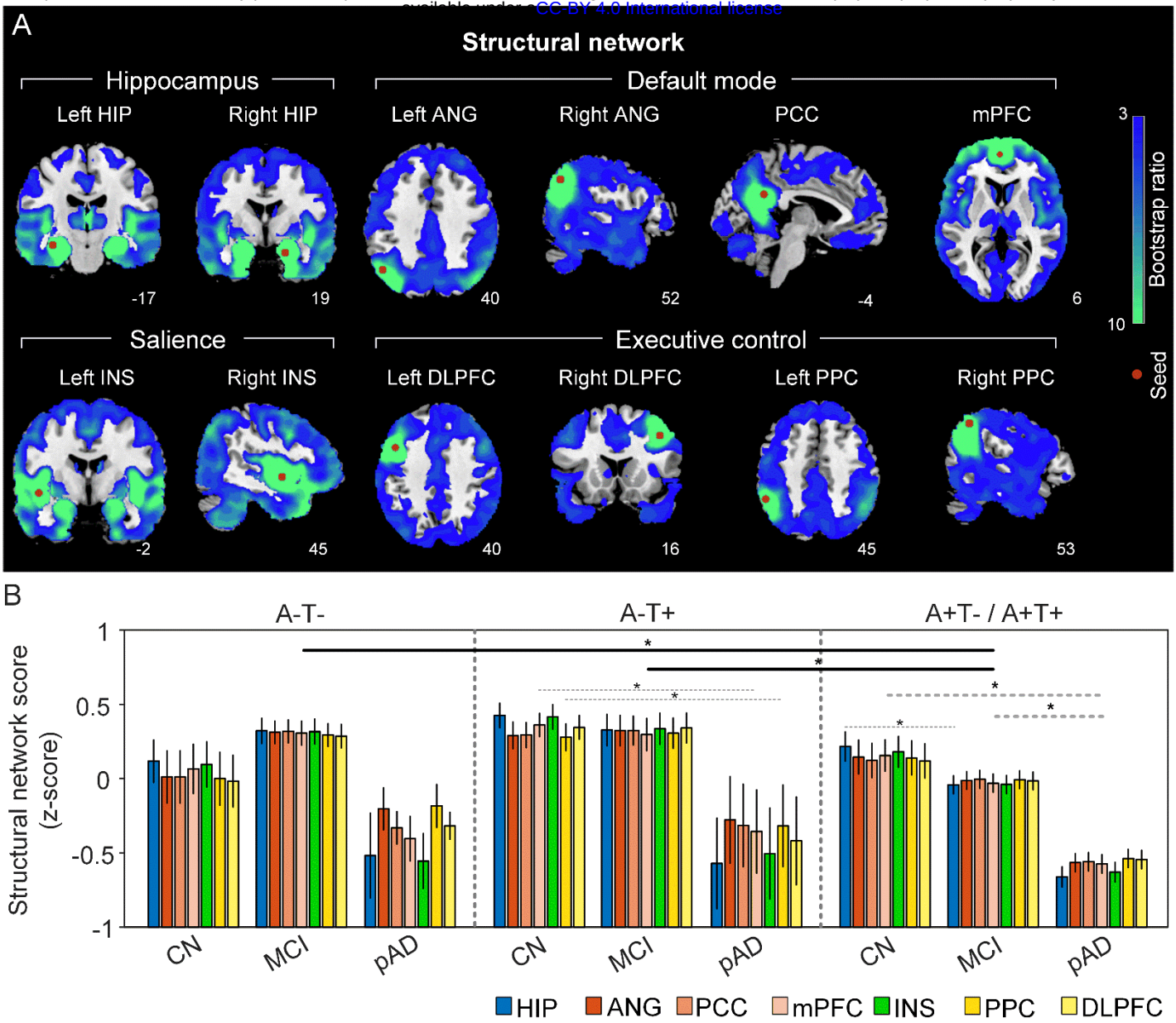

Supplementary Figure 3. The integrity of brain structural networks in participants with and without amyloid pathology across cognitive stages (validation dataset). A. brain slices of structural covariance networks associated with each brain seed defined from GMV data highlighted in blue circles. The intensity of colorbar represents bootstrap ratios, derived from dividing the weight of the singular-vector by the bootstrapped standard error. B. Individual-level brain structural network scores were lower in individuals with worse cognition and amyloid pathology. Summary of individual-level structural network scores (mean ± SD) were presented in bar charts. '*' indicates significant group difference (ANOVA; $p<0.05$). Thick lines indicate group differences in all brain network scores between different cognitive stages (grey dashed) or pathology groups (dark). Abbreviations: HIP = hippocampus; ANG = angular gyrus; PCC = posterior cingulate cortex; mPFC = media prefrontal cortex; INS = insular; DLPFC = dorsolateral prefrontal cortex; PPC = posterior parietal cortex; CN = cognitively normal; MCI = mild cognitive impairment; pAD = probable AD; A= β-amyloid; T = tau; '+'

= positive; '-' = negative; HIP = hippocampus; ANG = angular gyrus; PCC = posterior cingulate cortex; mPFC = media prefrontal cortex; INS = insular; DLPFC = dorsolateral prefrontal cortex; PPC = posterior parietal cortex.

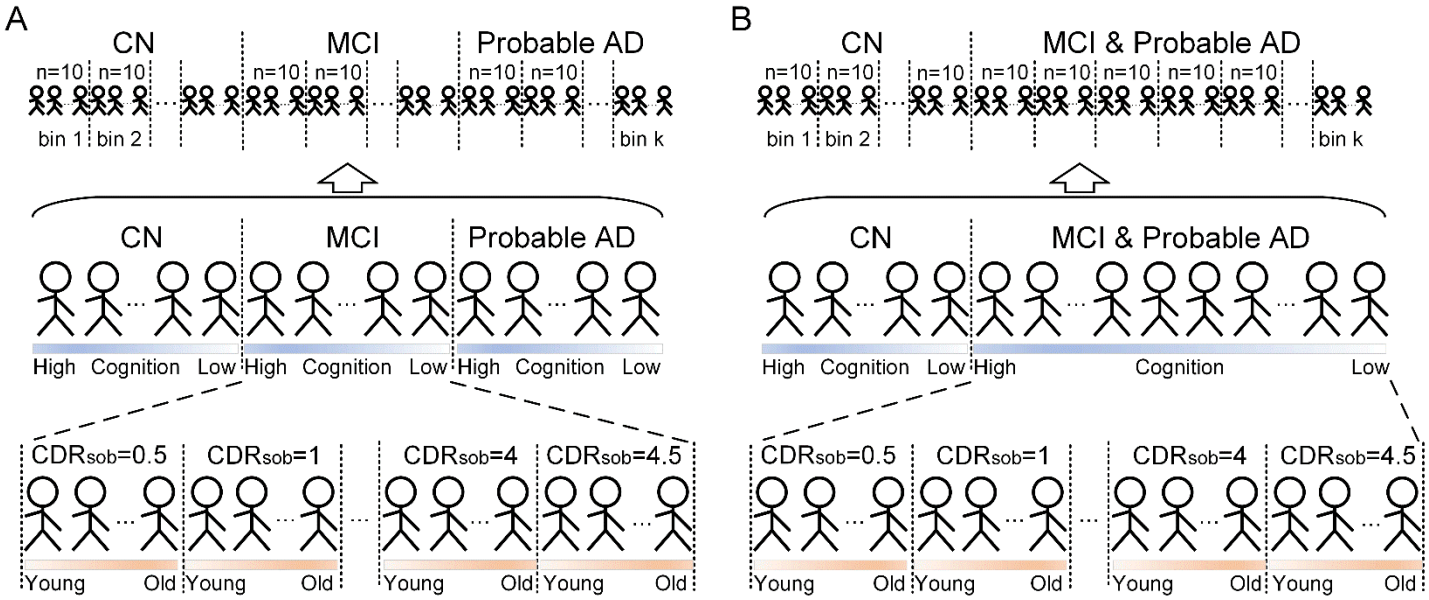

Supplementary Figure 4. Subject ordering for SVC modelling within each pathology group. The participants were ordered by their diagnosis. In the main ordering method (panel A), CN was followed by MCI, and MCI was followed by probable AD. The validation ordering method (panel B) did not differentiate MCI and probable, where CN subjects was followed by subjects with MCI or probable AD. Within each diagnosis, the participants were ordered by the severity of cognitive impairment (i.e., no impairment → severe impairment). Specifically, the participants within CN diagnosis were ordered by decreasing MMSE scores, and the participants within MCI or dementia diagnosis were ordered by increasing CDR-sum of boxes (SOB) scores. If the participants had the same MMSE or CDR-SOB scores in the earlier ordering step, they will then be further ordered by increasing age (i.e., young → old). After ordering the participants, we distributed the participants evenly into bins (i.e., 10 subjects/bin).

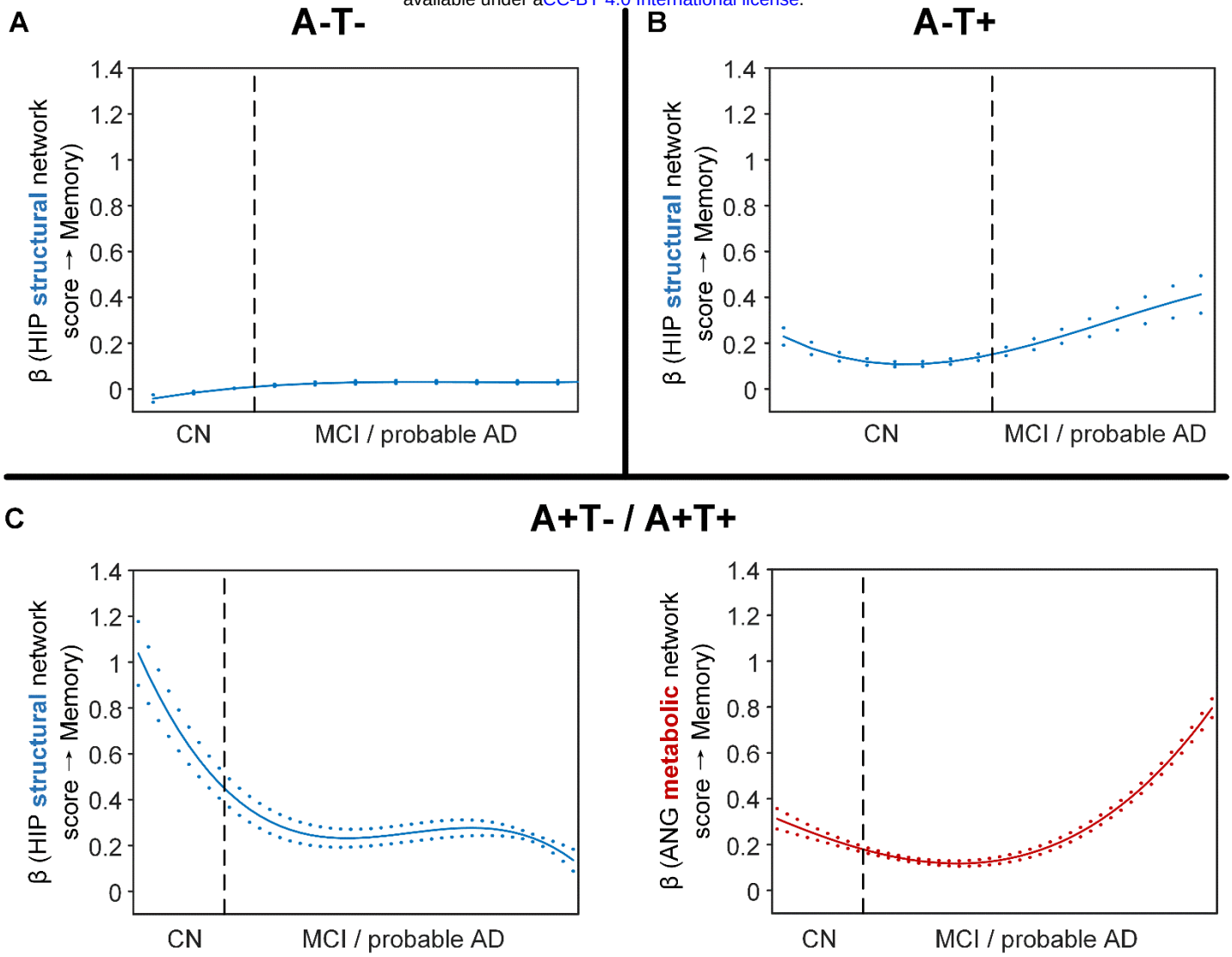

Supplementary Figure 5. Differential stage-dependent associations of metabolic and structural network scores with memory impairment in different pathology groups (main dataset with the alternative ordering strategy of treating MCI and probable AD as one group). Solid curves represent the mean associations (beta coefficients) of brain network scores with memory as a function of advancing AD continuum estimated from 100 replicates (metabolic in red; structural in blue). The dashed curves represent the point-wise 2* standard errors of the solid curves estimated from 100 replicates. The participants were ordered by their cognitive stages (i.e., CN → MCI/probable AD). Within each of the two stages, the participants were then ordered by general cognition or dementia severity (i.e., no impairment → severe impairment). Participants with the same cognitive impairment severity were further ordered by increasing age (i.e., young → old). Ordered participants were distributed evenly into bins (i.e., 10 subjects/bin). Abbreviations: CN = cognitively normal; MCI = mild cognitive impairment.

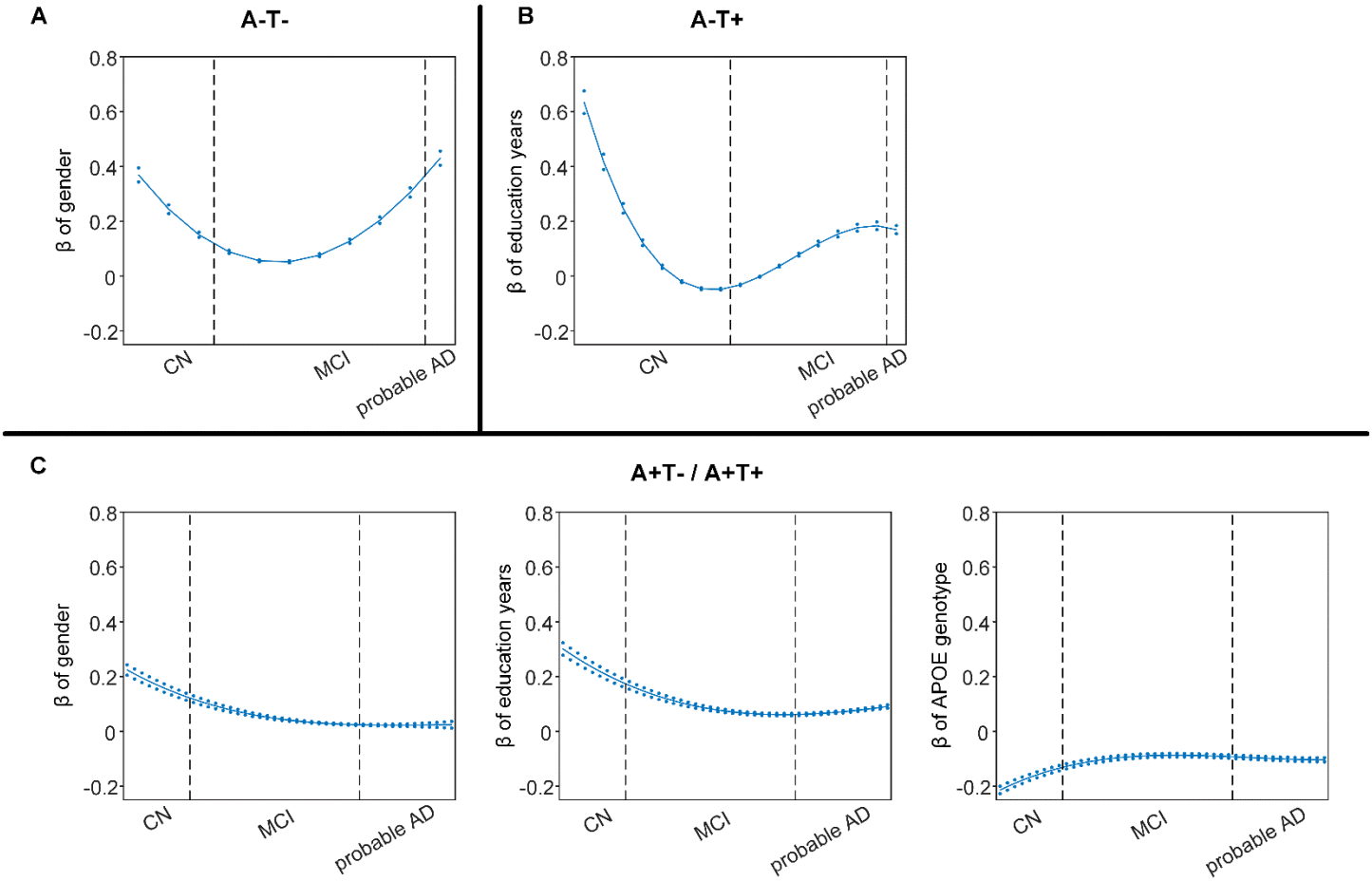

Supplementary Figure 6. Differential stage-dependent associations of demographic variables with memory impairment in different pathology groups (main dataset). Solid curves represent the mean associations (beta coefficients) of brain network scores with memory as a function of advancing AD continuum estimated from 100 replicates. The dashed curves represent the point-wise 2* standard errors of the solid curves estimated from 100 replicates. The participants were ordered by their cognitive stages (i.e., CN → MCI → probable AD). Within each diagnosis, the participants were then ordered by general cognition or dementia severity (i.e., no impairment → severe impairment). Participants with the same cognitive impairment severity were further ordered by increasing age (i.e., young → old). Ordered participants were distributed evenly into bins (i.e., 10 subjects/bin). Abbreviations: CN = cognitively normal; MCI = mild cognitive impairment.

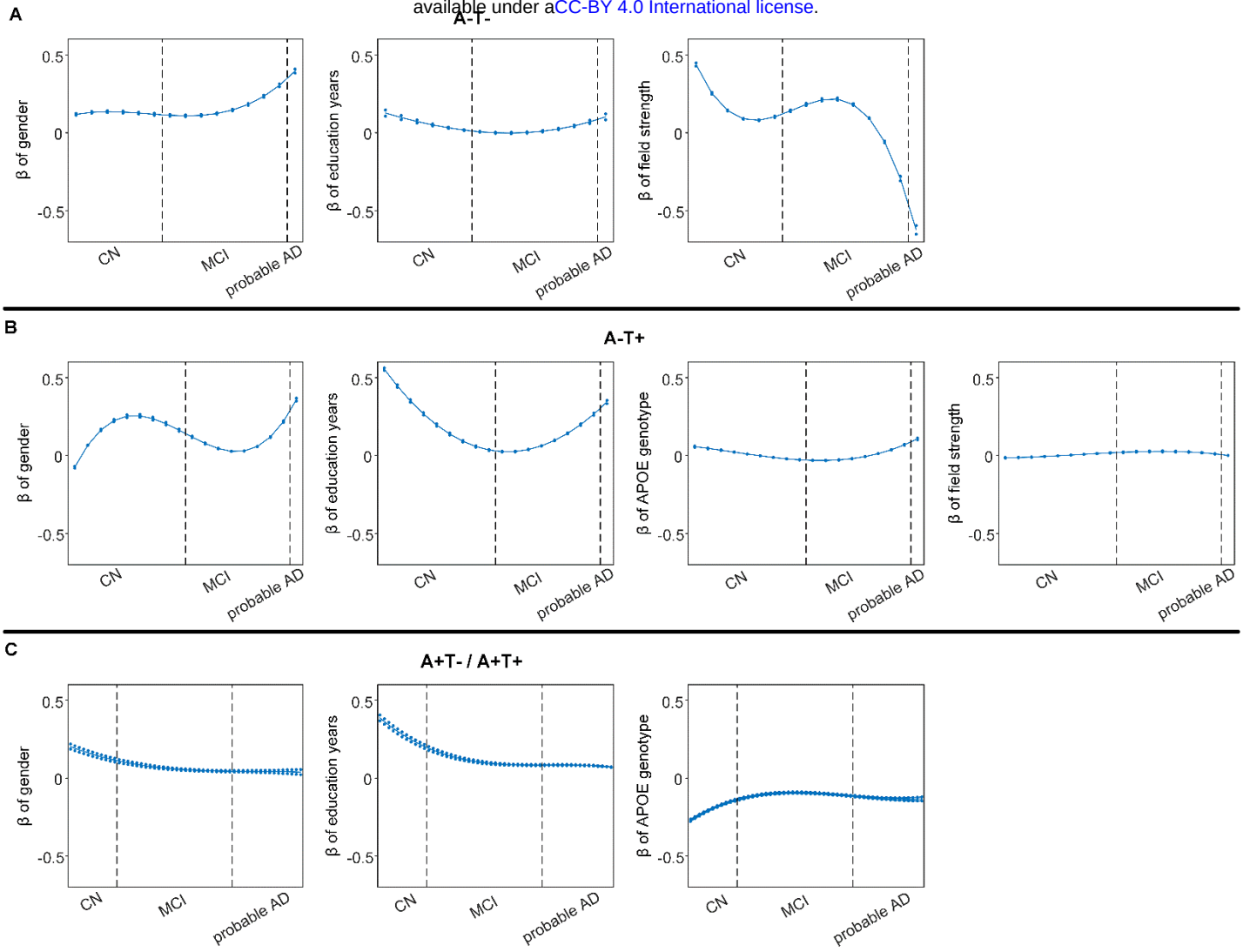

Supplementary Figure 7. Differential stage-dependent associations of demographical variables with memory impairment in different pathology group (validation dataset). Solid curves represent the mean associations (beta coefficients) of brain network scores with memory as a function of advancing AD continuum estimated from 100 replicates. The dashed curves represent the point-wise 2* standard errors of the solid curves estimated from 100 replicates. The participants were ordered by their cognitive stages (i.e., CN → MCI → probable AD). Within each diagnosis, the participants were then ordered by general cognition or dementia severity (i.e., no impairment → severe impairment). Participants with the same cognitive impairment severity were further ordered by increasing age (i.e., young → old). Ordered participants were distributed evenly into bins (i.e., 10 subjects/bin). Abbreviations: CN = cognitively normal; MCI = mild cognitive impairment.

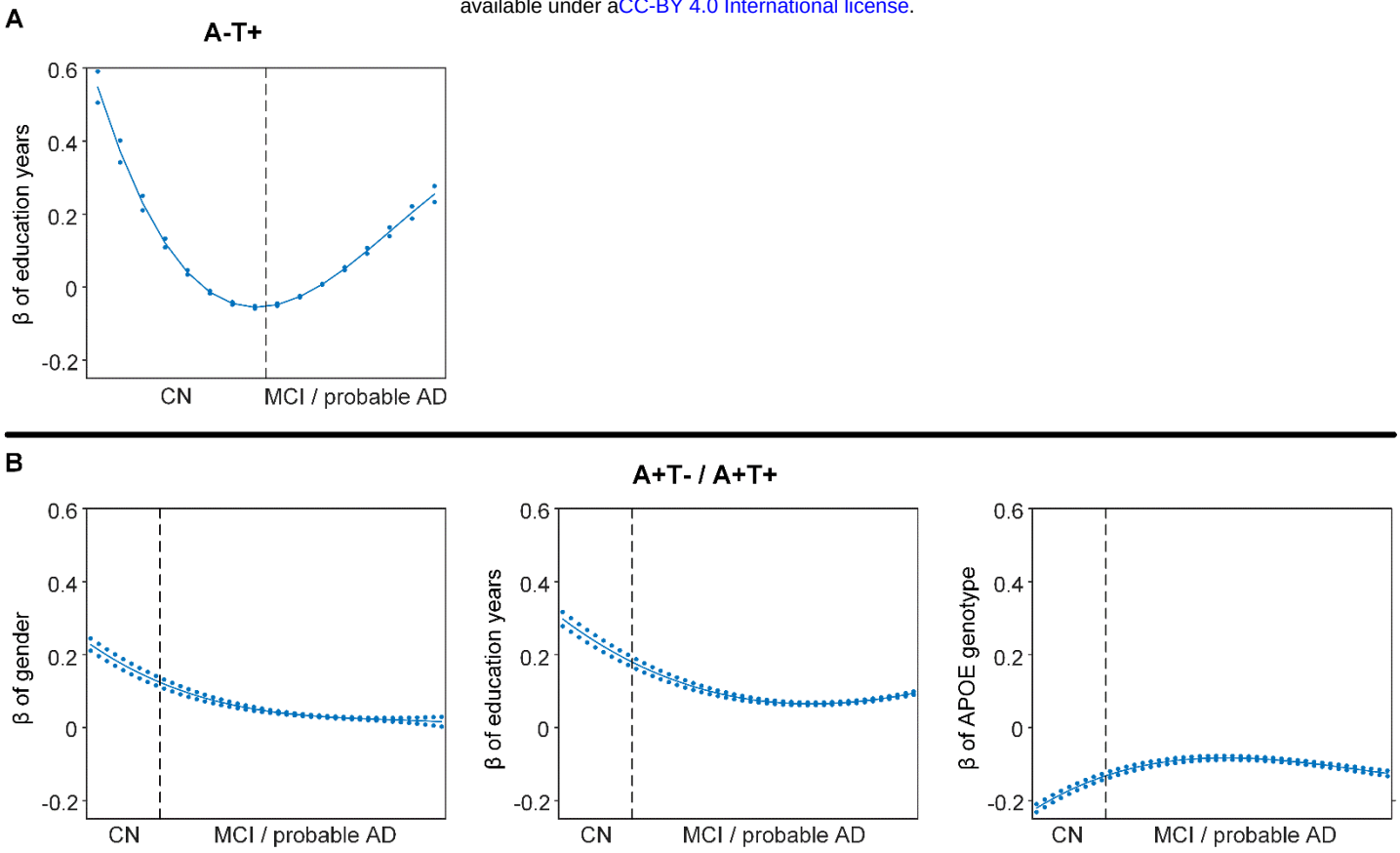

Supplementary Figure 8. Differential stage-dependent associations of demographical variables with memory impairment in different pathology group (main dataset with the ordering strategy merging the MCI and probable AD). Solid curves represent the mean associations (beta coefficients) of brain network scores with memory as a function of advancing AD continuum estimated from 100 replicates. The dashed curves represent the point-wise 2* standard errors of the solid curves estimated from 100 replicates. The participants were ordered by their cognitive stages (i.e., CN → MCI/ probable AD). Within each stage, the participants were then ordered by general cognition or dementia severity (i.e., no impairment → severe impairment). Participants with the same cognitive impairment severity were further ordered by increasing age (i.e., young → old). Ordered participants were distributed evenly into bins (i.e., 10 subjects/bin). Abbreviations: CN = cognitively normal; MCI = mild cognitive impairment.

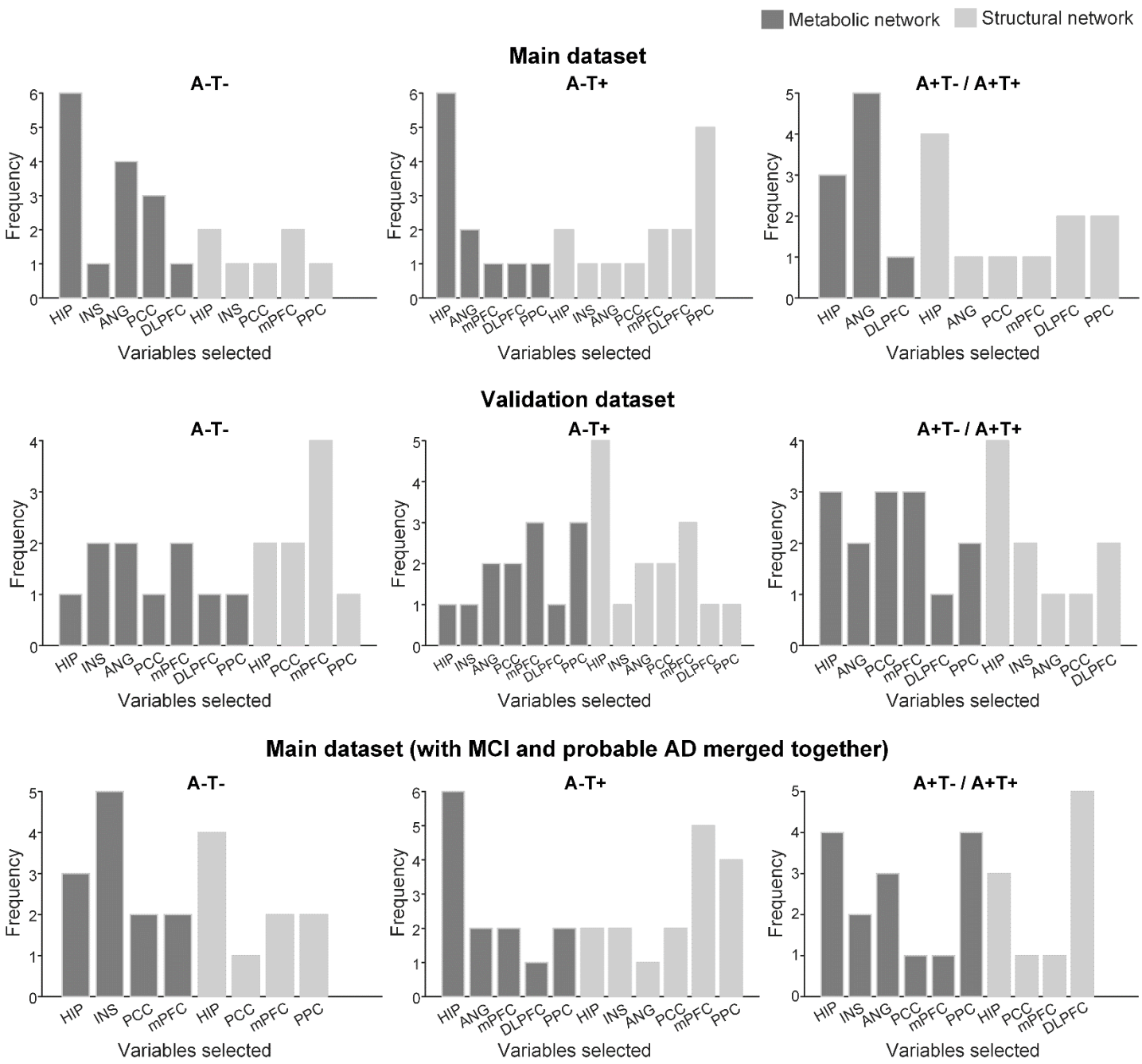

Supplementary Figure 9. Variable selection frequency distribution for permuted datasets using sparse varying-coefficient (SVC) model.